

EFFICIENT AND SIMPLE FOURTH-ORDER COMPACT FINITE DIFFERENCE METHODS FOR CONVECTION-DIFFUSION-REACTION EQUATIONS ON ARBITRARY CURVED DOMAINS

QIWEI FENG, BIN HAN, AND PETER MINEV

ABSTRACT. In this paper, we discuss the 2D convection-diffusion-reaction equation with variable smooth coefficients and the Dirichlet boundary condition on a complicated, thin, and curved domain. We propose the fourth-order compact FDM at every grid point with the uniform Cartesian mesh. For the regular stencil center, we utilize the fourth-order compact 9-point FDM to approximate the solution. According to the preliminary analysis, we use vertical and horizontal transformations to derive fourth-order compact FDMs in 10 cases for all irregular stencil centers. To obtain the left-hand side of the stencil of the fourth-order FDM in each case, we only need to solve an at most 6×24 linear system which is presented with the explicit formula. The right-hand side of the FDM is constructed in explicit expression for any irregular stencil centers too. To achieve the fourth-order consistency, up to second-order partial derivatives of convection, diffusion, reaction, and source terms are used for the FDM at the regular stencil center, and the FDM at an irregular stencil center only requires first-order partial derivatives of convection, diffusion, reaction, and source terms, and up to third-order derivatives of the Dirichlet boundary function and the parametric expression of the boundary curve. We test challenging domains with 100-leaf, high-curvature, high-frequency, sharply varying, and nearly overlapping boundary curves, the proposed FDM produces the high accuracy and the stable fourth-order convergence rate in l_2 and l_∞ norms. From error plots, we observe that errors are uniformly distributed on the closure of domains which confirms the robustness and stability. All examples numerically indicate that the accuracy and convergence rate seem to be independent of the distance between the boundary and the irregular stencil center when the mesh size h is reasonably small. All stencils of our FDMs have a simple desired structure by only keeping grid points inside Ω in the standard compact 9-point stencil for both regular stencils and boundary stencils, but without assuming any information outside the domain Ω .

AMS subject classifications: 65N06, 41A58.

Key words: Fourth-order compact FDM, simple compact stencil, variable coefficients, complicated thin domain, sharply varying boundary, efficient implementation.

1. INTRODUCTION

Partial differential equations (PDEs) on the complex irregular domain with the arbitrary geometry arise in many scientific and engineering applications. Typical examples include the fluid flow over the arbitrary domain, the heat transfer in the heterogeneous material, the free boundary problem, the parabolic moving boundary problem, and the diffusion process around the boundary with the irregular geometry. The complicated geometry of the irregular domain significantly increases the computational cost to obtain the accurate solution, because the sharply varying boundary requires very fine mesh. So in this paper, we derive the high-order finite difference method (FDM) to handle the arbitrary curved boundary. Since this paper focuses on FDMs, we mainly review the following literature of deriving efficient FDMs for various crucial PDEs over irregular domains, other numerical methods can be found in the references therein.

Arias et al. in [1] proposed the conservative method with the second-order accuracy for $-\nabla \cdot (\alpha \nabla u) = \phi$ with the constant diffusion term α and the Robin boundary condition $\rho u + \alpha \frac{\partial u}{\partial n} = g$ on the 2D irregular domain. Artzi et al. in [2] proved the second-order convergence rate of a compact FDM for the biharmonic equation on the 2D planar irregular domain. Baeza et al. in [3] constructed the high-order extrapolation technique of the weighted essentially non-oscillatory (WENO) FDM at the boundary of the 2D complex domain for the hyperbolic conservation law. The second-order unified FDM to solve the Poisson equation and the heat transfer problem with Dirichlet, Neumann, and Robin boundary conditions on the 2D irregular domain was discussed by Chai et al. in [5].

The fast second-order FDM for the biharmonic equation on the 2D irregular domain was derived by Chen et al. in [6]. The second-order FDM for variable coefficient Poisson and heat equations with the Dirichlet boundary condition using the non-graded adaptive grid on 2D and 3D irregular domains was established by Chen et al. in [7]. Clain et al. proposed the arbitrary high-order FDM for the linear convection-diffusion equation [8] and the nonlinear convection-diffusion-reaction equation [9] with Dirichlet, Neumann, linear or nonlinear Robin conditions on the arbitrary smooth 2D domain. Ding et al. applied the stencil-adaptive FDM to solve the 2D unsteady incompressible viscous flow with the curved boundary in [10]. The fourth-order embedded FDM for the 2D initial boundary value problem with the moving boundary and the Dirichlet boundary condition was built by Ditkowski et al. in [11]. Fidalgo et al. in [17] proposed the fifth-order WENO FDM with the ghost cell method to approximate the solution of the conservation law on the curved boundary domain. The fourth-order FDM for Laplace and heat equations with the Dirichlet boundary condition on the 2D arbitrary domain was designed by Gibou et al. in [18]. The second-order symmetric FDM for variable coefficient Poisson and heat equations with the Dirichlet boundary condition on 2D and 3D irregular domains was presented by Gibou et al. in [19]. Han et al. in [20] introduced the sixth-order compact FDM for the variable coefficient Poisson equation with the Dirichlet boundary condition on the 2D curved domain, and provided the corresponding convergence analysis. Helgadóttir et al. in [21] deduced the second-order FDM for the nonlinear Poisson-Boltzmann equation with Neumann or Robin boundary condition on 2D and 3D irregular domains with the arbitrary geometry using the non-graded adaptive grid, and the corresponding linear system in [21] to compute the solution is symmetric positive definite if the uniform grid is applied. By employing 1 to 4 points at the boundary, Ito et al. in [22] developed the fourth-order compact FDM or immersed interface method (IIM) for the diffusion-reaction equation on the irregular domain with the Robin boundary condition, and Li et al. in [25] derived the fourth-order compact FDM/IIM for Poisson and heat equations on the 2D irregular domain with the Dirichlet boundary condition (necessary steps are provided to deal with the 3D irregular domain). The embedded FDM for the Poisson equation with the Dirichlet boundary condition on the 2D irregular domain was proposed by Jomaa et al. in [23]. Lakner et al. in [24] established the efficient symbolic-numerical procedure of the FDM for Laplace and heat equations with Dirichlet and Neumann boundary conditions over the 2D curvilinear domain. Li et al. in [26, 27] formulated the fourth-order in space and the second-order in time augmented matched interface and boundary (AMIB) method with the Fast Sine or Fast Fourier Transform acceleration for elliptic and/or parabolic problems over 2D and/or 3D irregular domains with Dirichlet, Neumann, and Robin boundary conditions. Liszka et al. in [28] applied the FDM with the arbitrary irregular grid to solve the applied mechanics problem. Ng et al. in [29] proposed the second-order ghost fluid method for the variable coefficient Poisson equation with the Dirichlet boundary condition on 2D and 3D irregular domains. Olsson in [30] derived the FDM with the third-order accuracy at the boundary and the sixth-order accuracy in the interior domain for parabolic and symmetric hyperbolic systems over the non-smooth domain. Pan et al. in [31] developed an augmented third-order compact FDM/IIM for the Poisson/Helmholtz equation with Dirichlet, Neumann, and Robin boundary conditions on the 2D irregular domain. The fourth-order AMIB method with the FFT acceleration for $\Delta u + \kappa u = \phi$ with the boundary condition $\rho u + \zeta \frac{\partial u}{\partial n} = g$ on 2D and 3D irregular domains was established by Ren et al. in [32]. The sharp second-order finite volume and difference method with the adaptive grid for the linear elasticity equation with Dirichlet and Neumann boundary conditions on 2D and 3D irregular domains was constructed by Theillard et al. in [34]. Yoon et al. in [35] derived the second-order convergence proof of the FDM proposed by Gibou et al. for the Poisson equation with the Dirichlet boundary condition on the 2D irregular domain. The second-order augmented IIM for the Helmholtz/Poisson equation with the Dirichlet boundary condition on the 2D irregular domain in complex space was built by Zhang et al. in [36]. For the convergence proof of the high-order compact FDM over rectangular and cubic domains, Berikelashvili et al. in [4] provided the convergence proof of the fourth-order compact FDM for the convection-diffusion equation with the constant coefficient and the Dirichlet boundary condition in the unit cube, and Shi et al. in [33] proved the stability

and the optimal fourth-order convergence rate of the compact block-centered FDM for elliptic and parabolic problems with the variable coefficient on the rectangular domain.

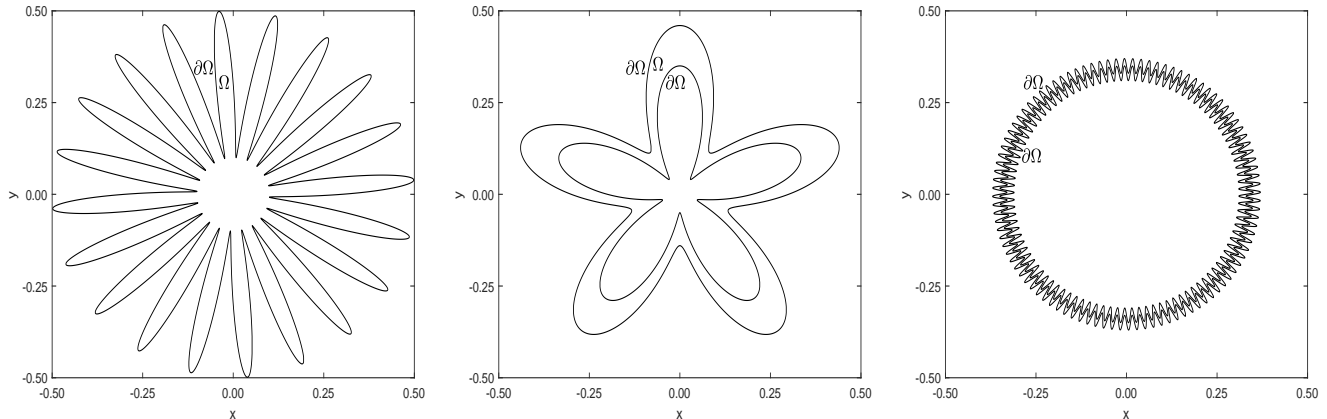


FIGURE 1. Three examples of Ω with complicated boundary curves $\partial\Omega$ for the model problem (1.1): Ω is the region enclosed by a 20-leaf boundary curve (left), Ω is the region enclosed by two 5-leaf boundary curves (middle), and Ω is the thin region enclosed by two 100-leaf boundary curves (right).

In this paper, we derive the fourth-order compact finite difference method (FDM) to solve the 2D convection-diffusion-reaction equation with the Dirichlet boundary condition on an arbitrary irregular domain $\Omega \subset \mathbb{R}^2$ with the smooth boundary curve $\partial\Omega$ as follows:

$$\begin{cases} -\nabla \cdot (\alpha \nabla u) + \vec{\beta} \cdot \nabla u + \kappa u = \phi, & (x, y) \in \Omega, \\ u = g, & (x, y) \in \partial\Omega, \end{cases} \quad (1.1)$$

where $\alpha > 0$, $\vec{\beta} = (\beta_1, \beta_2)$, κ , and ϕ are variable functions in $\bar{\Omega}$. See Fig. 1 for illustrations of Ω that we discuss in this paper to construct the fourth-order compact FDM to solve (1.1). To derive the fourth-order compact FDM, we assume that

- the partial derivatives of u up to the fourth order are uniformly continuous on $\bar{\Omega}$,
- the partial derivatives of α , $\vec{\beta}$, κ , and ϕ up to the second order are uniformly continuous on $\bar{\Omega}$,
- the derivatives of the Dirichlet boundary function g and the parametric expression of the boundary curve $\partial\Omega$ up to the third order are uniformly continuous on $\partial\Omega$.

Let

$$a := \frac{\alpha_x - \beta_1}{\alpha}, \quad b := \frac{\alpha_y - \beta_2}{\alpha}, \quad d := -\frac{\kappa}{\alpha}, \quad f := -\frac{\phi}{\alpha}. \quad (1.2)$$

Then (1.1) implies

$$\Delta u + au_x + bu_y + du = f. \quad (1.3)$$

For simplification, we assume that the original point $(0, 0) \in \Omega$ to describe the uniform Cartesian grid used in this paper for Ω :

$$(x_i, y_j) \cap \bar{\Omega} \quad \text{with} \quad (x_i, y_j) := (ih, jh), \quad i, j = 0, \pm 1, \pm 2, \dots, \quad \text{and} \quad h := 1/N, \quad N \in \mathbb{N}. \quad (1.4)$$

We also define that

$$u_{i,j} = u(x_i, y_j), \quad (u_h)_{i,j} = \text{the value of } u_h \text{ that computed at the grid point } (x_i, y_j),$$

where u_h is the numerical solution that approximated by our proposed fourth-order compact FDM for (1.1). Furthermore, we say that the compact FDM utilizes the regular stencil at the center point (x_i, y_j) if $\{(x_{i+\mu}, y_{j+\nu}) : -1 \leq \mu, \nu \leq 1\} \in \bar{\Omega}$ with (x_i, y_j) denoting the regular stencil center (see blue points in the left panel of Fig. 2 for illustrations), otherwise the compact FDM utilizes the irregular stencil with (x_i, y_j) denoting the irregular stencil center (see red points in the left panel of Fig. 2 for illustrations).

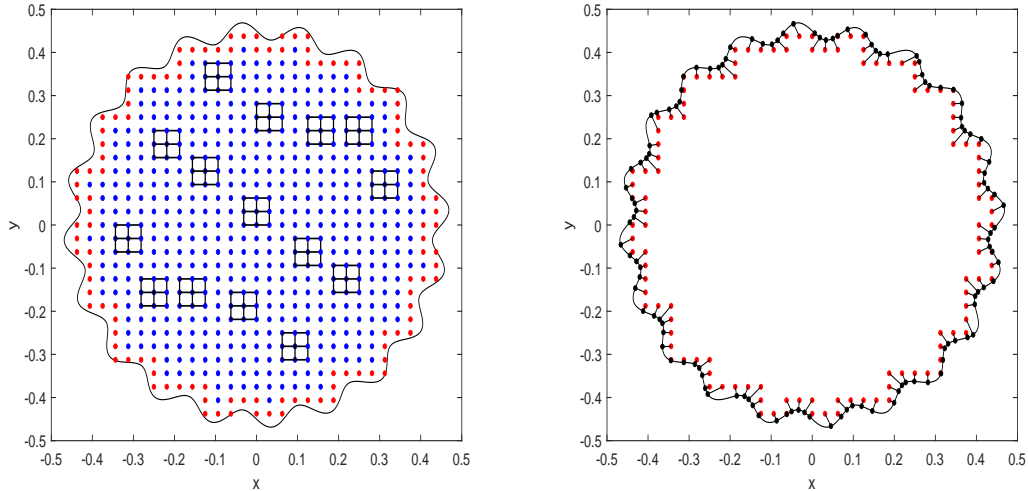


FIGURE 2. Left: Regular (blue) and irregular (red) stencil centers. Right: Orthogonal projections (black points) of the stencil centers (red points) of boundary irregular stencils onto the boundary curve $\partial\Omega$ (the black curve).

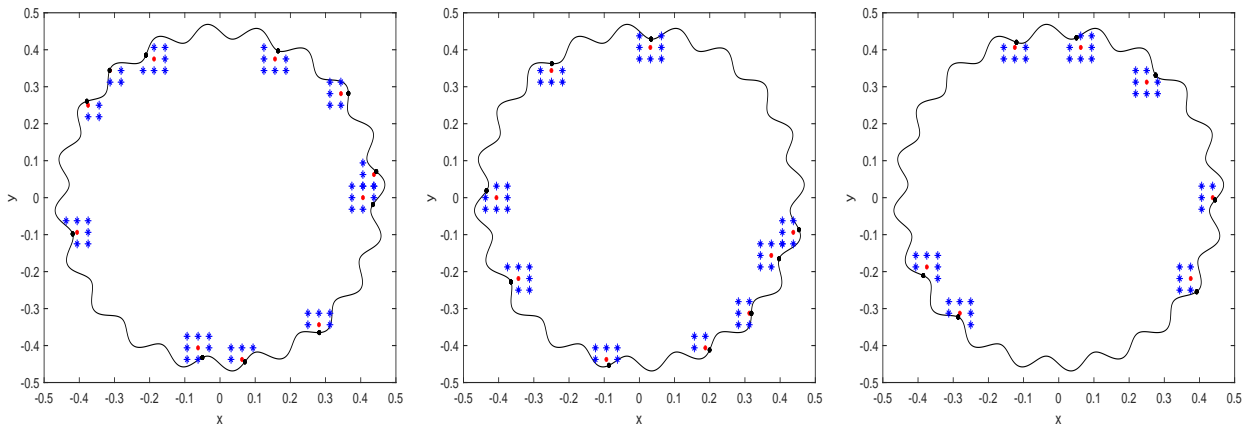


FIGURE 3. Illustrations for compact FDMs at irregular stencil centers, where each red point is the stencil center of a boundary irregular stencil near $\partial\Omega$, a black point is the orthogonal projection of the stencil center of the boundary stencil onto $\partial\Omega$, the blue star points are remaining grid points used in compact FDMs, and the black curve is the boundary $\partial\Omega$.

This paper is organized as following: In Section 2, we provide the fourth-order compact 9-point FDM at the regular stencil center point. In Section 3, we derive the fourth-order compact FDM at the irregular stencil center point in 10 cases. Since the stencil of the compact FDM at the irregular stencil center point has various configurations (see Fig. 3 for illustrations) for the complex boundary curve, it is hard to derive the corresponding FDM for every configuration. We present an at most 6 times 24 linear system with the explicit expression to compute the left-hand side of the stencil of the fourth-order compact FDM for any irregular stencil center points. Once the left-hand side of the FDM is determined, the right-hand side is calculated directly by its explicit formula. In Section 4, we test 3 examples with complicated curved boundaries to verify convergence rates of errors in l_2 and l_∞ norms of the proposed FDM. In Section 5, the main contribution is summarized.

2. FOURTH-ORDER COMPACT FDM AT THE REGULAR STENCIL CENTER POINT

In this section, we use the fourth-order compact 9-point FDM that proposed in [16, Theorem 2.1] to compute u_h to approximate u at the regular stencil center point (x_i, y_j) .

Theorem 2.1. *Let $\alpha > 0, \vec{\beta}, \kappa, \phi, u$ be smooth in $\bar{\Omega}$ in (1.1), $\partial\Omega$ be a smooth boundary curve, and functions a, b, d, f be defined in (1.2). Then the following compact 9-point FDM [16, Theorem 2.1] (see the left panel of Fig. 2 for illustrations)*

$$\mathcal{L}_h(u_h)_{i,j} := \frac{1}{h^2} \sum_{r,\ell=-1}^1 C_{r,\ell} \Big|_{(x,y)=(x_i,y_j)} (u_h)_{i+r,j+\ell} = F_{i,j} \Big|_{(x,y)=(x_i,y_j)}, \quad (2.1)$$

achieves the fourth-order consistency for (1.1) at the regular stencil center point (x_i, y_j) , where

$$\begin{aligned} C_{-1,-1} &:= \frac{1}{6} - \frac{a+b}{12}h, \\ C_{-1,0} &:= \frac{2}{3} - \frac{a}{3}h + \frac{1}{12}[a^2 + ab + d + 2a_x + a_y + b_x]h^2 \\ &\quad - \frac{1}{24}[a(a_x + d) + ba_y + 2d_x + \Delta a]h^3, \\ C_{-1,1} &:= \frac{1}{6} - \frac{1}{12}[a - b]h - \frac{1}{12}[ab + a_y + b_x]h^2, \\ C_{0,-1} &:= \frac{2}{3} - \frac{b}{3}h + \frac{1}{12}[b^2 + ab + a_y + b_x + 2b_y + d]h^2 \\ &\quad - \frac{1}{24}[ab_x + b(b_y + d) + 2d_y + \Delta b]h^3 + \frac{bd_y}{12}h^4, \\ C_{0,0} &:= \frac{-10}{3} - \frac{1}{6}[a^2 + ab + b^2 - 4d + 2a_x + a_y + b_x + 2b_y]h^2 \\ &\quad + \frac{1}{12}[ad_x + \Delta d]h^4, \\ C_{0,1} &:= \frac{2}{3} + \frac{b}{3}h + \frac{1}{12}[ab + b^2 + d + a_y + b_x + 2b_y]h^2 \\ &\quad + \frac{1}{24}[ab_x + b(b_y + d) + 2d_y + \Delta b]h^3, \\ C_{1,-1} &:= \frac{1}{6} + \frac{1}{12}[a - b]h - \frac{1}{12}[ab + a_y + b_x]h^2 - \frac{bd_y}{12}h^4, \\ C_{1,0} &:= \frac{2}{3} + \frac{a}{3}h + \frac{1}{12}[a^2 + ab + d + 2a_x + a_y + b_x]h^2 \\ &\quad + \frac{1}{24}[a(a_x + d) + ba_y + 2d_x + \Delta a]h^3 + \frac{bd_y}{12}h^4, \\ C_{1,1} &:= \frac{1}{6} + \frac{1}{12}[a + b]h, \end{aligned} \quad (2.2)$$

and

$$F_{i,j} := f + \frac{1}{12}[af_x + bf_y + \Delta f]h^2. \quad (2.3)$$

By (1.2), (2.2), and (2.3), the first-order and second-order partial derivatives of $\alpha, \vec{\beta}, \kappa, \phi$ in (1.1) are sufficient to attain the fourth-order consistency of the compact 9-point FDM at the regular stencil center point in Theorem 2.1.

3. FOURTH-ORDER COMPACT FDM AT AN IRREGULAR STENCIL CENTER POINT

In this section, we propose the fourth-order compact FDM at an irregular stencil center point. For simplification, we assume that the parametric equation of the boundary curve $\partial\Omega$ satisfies

$$(x, y) = (x(t), y(t)) = (p(t), q(t)), \quad \text{for } (x, y) \in \partial\Omega. \quad (3.1)$$

Then the Dirichlet boundary condition in (1.1) results in

$$u(x(t), y(t)) = g(t), \quad (x(t), y(t)) \in \partial\Omega. \quad (3.2)$$

For the irregular stencil center point (x_i, y_j) , we define that

$$u^{(m,n)} := \frac{\partial^{m+n} u(x, y)}{\partial x^m \partial y^n} \Big|_{(x,y)=(x_i^o, y_j^o)}, \quad (3.3)$$

$$a^{(m,n)} := \frac{\partial^{m+n} a(x, y)}{\partial x^m \partial y^n} \Big|_{(x,y)=(x_i^o, y_j^o)}, \quad b^{(m,n)} := \frac{\partial^{m+n} b(x, y)}{\partial x^m \partial y^n} \Big|_{(x,y)=(x_i^o, y_j^o)}, \quad (3.4)$$

$$d^{(m,n)} := \frac{\partial^{m+n} d(x, y)}{\partial x^m \partial y^n} \Big|_{(x,y)=(x_i^o, y_j^o)}, \quad f^{(m,n)} := \frac{\partial^{m+n} f(x, y)}{\partial x^m \partial y^n} \Big|_{(x,y)=(x_i^o, y_j^o)}, \quad (3.5)$$

where a, b, d, f are defined in (1.2), and (x_i^o, y_j^o) is the orthogonal projection on $\partial\Omega$ of the irregular stencil center point (x_i, y_j) (see black points in Fig. 2 and Fig. 3 for illustrations).

We also assume that there exists t_k^o such that

$$(x_i^o, y_j^o) = (p(t_k^o), q(t_k^o)) \quad \text{for some } k \quad \text{with} \quad [p'(t_k^o)]^2 + [q'(t_k^o)]^2 \neq 0, \quad (3.6)$$

and

$$p^{(m)} := \left. \frac{d^m p(t)}{dt^m} \right|_{t=t_k^o}, \quad q^{(m)} := \left. \frac{d^m q(t)}{dt^m} \right|_{t=t_k^o}, \quad g^{(m)} := \left. \frac{d^m g(t)}{dt^m} \right|_{t=t_k^o}. \quad (3.7)$$

From our high-order FDM on the rectangle domain in [12, 14], we need to use vertical and horizontal transformations for vertical and horizontal boundaries, respectively. As $q^{(1)}/p^{(1)}$ is the slope of the tangent line of the boundary curve $\partial\Omega$, the tangent line is close to the vertical boundary case if $|q^{(1)}/p^{(1)}| \geq 1$, and the tangent line is close to the horizontal boundary case if $|q^{(1)}/p^{(1)}| \leq 1$. So we use the vertical transformation for $|q^{(1)}/p^{(1)}| \geq 1$ and the horizontal transformation for $|q^{(1)}/p^{(1)}| \leq 1$ naturally.

Based on the preliminary analysis, to propose the fourth-order compact FDM at all irregular stencil center points, we need to consider 10 subcases of 2 cases ($|q^{(1)}/p^{(1)}| \geq 1$ and $|q^{(1)}/p^{(1)}| \leq 1$). In this section, we provide the derivation of FDM for the subcase 1 of the case 1 in Theorem 3.1, and present the FDM for the subcase 1 of the case 2 directly in Theorem 3.2. For other 8 subcases, we give necessary details to help readers to derive corresponding FDMs straightforwardly. Furthermore, we also present Remark 3.3 to provide a feasible way to avoid 8 subcases, i.e., the FDMs in Theorems 3.1 and 3.2 can achieve the fourth-order consistency at any irregular stencil center points of all 10 subcases.

Case 1: $|q^{(1)}/p^{(1)}| \geq 1$. (1.3) yields

$$au^{(1,0)} + bu^{(0,1)} + du + u^{(2,0)} + u^{(0,2)} = f. \quad (3.8)$$

Differentiating (3.8) with respect to x and y , we obtain

$$au^{(2,0)} + a^{(1,0)}u^{(1,0)} + bu^{(1,1)} + b^{(1,0)}u^{(0,1)} + du^{(1,0)} + d^{(1,0)}u + u^{(1,2)} + u^{(3,0)} = f^{(1,0)}, \quad (3.9)$$

$$au^{(1,1)} + a^{(0,1)}u^{(1,0)} + bu^{(0,2)} + b^{(0,1)}u^{(0,1)} + du^{(0,1)} + d^{(0,1)}u + u^{(0,3)} + u^{(2,1)} = f^{(0,1)}. \quad (3.10)$$

Then (3.8)–(3.10) imply (see the first arrow in Fig. 4 for an illustration)

$$\begin{aligned} u^{(2,0)} &= -au^{(1,0)} - bu^{(0,1)} - du - u^{(0,2)} + f, \\ u^{(2,1)} &= -au^{(1,1)} - a^{(0,1)}u^{(1,0)} - bu^{(0,2)} - b^{(0,1)}u^{(0,1)} - du^{(0,1)} \\ &\quad - d^{(0,1)}u - u^{(0,3)} + f^{(0,1)}, \\ u^{(3,0)} &= a^2u^{(1,0)} + abu^{(0,1)} + adu - af + au^{(0,2)} - a^{(1,0)}u^{(1,0)} \\ &\quad - bu^{(1,1)} - b^{(1,0)}u^{(0,1)} - du^{(1,0)} - d^{(1,0)}u - u^{(1,2)} + f^{(1,0)}. \end{aligned} \quad (3.11)$$

Differentiating (3.2) with respect to t three times yields

$$\begin{aligned} u &= g, \\ p^{(1)}u^{(1,0)} + q^{(1)}u^{(0,1)} &= g^{(1)}, \\ [p^{(1)}]^2u^{(2,0)} + 2p^{(1)}q^{(1)}u^{(1,1)} + [q^{(1)}]^2u^{(0,2)} \\ &\quad + p^{(2)}u^{(1,0)} + q^{(2)}u^{(0,1)} &= g^{(2)}, \\ [p^{(1)}]^3u^{(3,0)} + 3[p^{(1)}]^2q^{(1)}u^{(2,1)} + 3p^{(1)}[q^{(1)}]^2u^{(1,2)} \\ &\quad + [q^{(1)}]^3u^{(0,3)} + 3p^{(1)}p^{(2)}u^{(2,0)} + 3p^{(1)}q^{(2)}u^{(1,1)} \\ &\quad + 3p^{(2)}q^{(1)}u^{(1,1)} + 3q^{(1)}q^{(2)}u^{(0,2)} + p^{(3)}u^{(1,0)} \\ &\quad + q^{(3)}u^{(0,1)} &= g^{(3)}. \end{aligned} \quad (3.12)$$

Substituting (3.11) into (3.12), then the symbolic calculation results in (see the second arrow in Fig. 4 for an illustration)

$$\begin{aligned}
u &= g, \\
u^{(0,1)} &= s_1 u^{(1,0)} - z_1 g^{(1)}, \\
u^{(0,2)} &= s_2 u^{(1,0)} + s_3 u^{(1,1)} - z_3 f - z_2 g - z_4 g^{(1)} - z_5 g^{(2)}, \\
u^{(0,3)} &= s_4 u^{(1,0)} + s_5 u^{(1,1)} + s_6 u^{(1,2)} - z_7 f - z_8 f^{(0,1)} \\
&\quad - z_{10} f^{(1,0)} - z_6 g - z_9 g^{(1)} - z_{11} g^{(2)} - z_{12} g^{(3)},
\end{aligned} \tag{3.13}$$

where

$$\begin{aligned}
s_1 &= -p^{(1)}/q^{(1)}, \\
s_2 &= \{b[p^{(1)}]^3 - a[p^{(1)}]^2 q^{(1)} - p^{(1)} q^{(2)} \\
&\quad + p^{(2)} q^{(1)}\} / \{q^{(1)}([p^{(1)}]^2 - [q^{(1)}]^2)\}, \\
s_3 &= 2q^{(1)} p^{(1)} / \{[p^{(1)}]^2 - [q^{(1)}]^2\}, \\
s_4 &= \{b^{(1,0)}[p^{(1)}]^6 - q^{(1)}(3b^2 + a^{(1,0)} - 3b^{(0,1)} \\
&\quad - 2d)[p^{(1)}]^5 + ([4ab - 3a^{(0,1)} - b^{(1,0)}][q^{(1)}]^2 \\
&\quad - aq^{(2)})[p^{(1)}]^4 + ([a^{(1,0)} - a^2 - 3b^{(0,1)} - 2d][q^{(1)}]^3 \\
&\quad + (ap^{(2)} + 6bq^{(2)})q^{(1)} - q^{(3)})[p^{(1)}]^3 + (3a^{(0,1)}[q^{(1)}]^4 \\
&\quad - (3aq^{(2)} + 6bp^{(2)})[q^{(1)}]^2 + p^{(3)}q^{(1)} + 3p^{(2)}q^{(2)})[p^{(1)}]^2 \\
&\quad + 3(ap^{(2)}[q^{(1)}]^2 - [p^{(2)}]^2 + q^{(1)}q^{(3)}/3 - [q^{(2)}]^2)q^{(1)}p^{(1)} \\
&\quad + 3p^{(2)}q^{(2)}[q^{(1)}]^2 - p^{(3)}[q^{(1)}]^3\} / \{[q^{(1)}]^2(3[p^{(1)}]^4 \\
&\quad - 4[p^{(1)}]^2[q^{(1)}]^2 + [q^{(1)}]^4)\}, \\
s_5 &= \{3a[p^{(1)}]^2[q^{(1)}]^3 - a[p^{(1)}]^4 q^{(1)} - b[p^{(1)}]^5 - 5b[p^{(1)}]^3[q^{(1)}]^2 \\
&\quad + 3[p^{(1)}]^3 q^{(2)} - 3[p^{(1)}]^2 p^{(2)} q^{(1)} + 3p^{(1)}[q^{(1)}]^2 q^{(2)} - 3p^{(2)}[q^{(1)}]^3\} \\
&\quad / \{q^{(1)}(3[p^{(1)}]^4 - 4[p^{(1)}]^2[q^{(1)}]^2 + [q^{(1)}]^4)\}, \\
s_6 &= -p^{(1)}\{[p^{(1)}]^2 - 3[q^{(1)}]^2\} / \{q^{(1)}(3[p^{(1)}]^2 - [q^{(1)}]^2)\},
\end{aligned} \tag{3.14}$$

and

$$\begin{aligned}
z_1 &= -1/q^{(1)}, \\
z_2 &= d[p^{(1)}]^2 / \{[p^{(1)}]^2 - [q^{(1)}]^2\}, \\
z_3 &= -[p^{(1)}]^2 / \{[p^{(1)}]^2 - [q^{(1)}]^2\}, \\
z_4 &= \{b[p^{(1)}]^2 - q^{(2)}\} / \{q^{(1)}([p^{(1)}]^2 - [q^{(1)}]^2)\}, \\
z_5 &= 1 / \{[p^{(1)}]^2 - [q^{(1)}]^2\}, \\
z_6 &= p^{(1)}\{d^{(1,0)}[p^{(1)}]^4 - 3q^{(1)}(bd - d^{(0,1)})[p^{(1)}]^3 + [q^{(1)}]^2(ad \\
&\quad - d^{(1,0)})[p^{(1)}]^2 + (3dq^{(1)}q^{(2)} - 3d^{(0,1)}[q^{(1)}]^3)p^{(1)} - 3dp^{(2)}[q^{(1)}]^2\} \\
&\quad / \{q^{(1)}(3[p^{(1)}]^4 - 4[p^{(1)}]^2[q^{(1)}]^2 + [q^{(1)}]^4)\}, \\
z_7 &= -p^{(1)}\{a[p^{(1)}]^2 q^{(1)} - 3b[p^{(1)}]^3 + 3p^{(1)}q^{(2)} - 3p^{(2)}q^{(1)}\} / \{3[p^{(1)}]^4 \\
&\quad - 4[p^{(1)}]^2[q^{(1)}]^2 + [q^{(1)}]^4\}, \\
z_8 &= -3[p^{(1)}]^2 / \{3[p^{(1)}]^2 - [q^{(1)}]^2\},
\end{aligned} \tag{3.15}$$

$$\begin{aligned}
z_9 &= \{b^{(1,0)}[p^{(1)}]^5 - 3q^{(1)}(b^2 - b^{(0,1)} - d)[p^{(1)}]^4 + ([ab - b^{(1,0)}][q^{(1)}]^2 \\
&\quad - aq^{(2)})[p^{(1)}]^3 + (6bq^{(1)}q^{(2)} - 3(d + b^{(0,1)})[q^{(1)}]^3 - q^{(3)})[p^{(1)}]^2 \\
&\quad - 3p^{(2)}(b[q^{(1)}]^2 - q^{(2)})p^{(1)} + q^{(3)}[q^{(1)}]^2 - 3q^{(1)}[q^{(2)}]^2\} \\
&\quad / \{[q^{(1)}]^2(3[p^{(1)}]^4 - 4[p^{(1)}]^2[q^{(1)}]^2 + [q^{(1)}]^4)\}, \\
z_{10} &= -[p^{(1)}]^3 / \{q^{(1)}(3[p^{(1)}]^2 - [q^{(1)}]^2)\}, \\
z_{11} &= \{a[p^{(1)}]^3 - 3b[p^{(1)}]^2q^{(1)} - 3p^{(1)}p^{(2)} + 3q^{(1)}q^{(2)}\} / \{q^{(1)}(3[p^{(1)}]^4 \\
&\quad - 4[p^{(1)}]^2[q^{(1)}]^2 + [q^{(1)}]^4)\}, \\
z_{12} &= 1 / \{q^{(1)}(3[p^{(1)}]^2 - [q^{(1)}]^2)\}.
\end{aligned}$$

From denominators of expressions in (3.14) and (3.15), we can say that s_1, \dots, s_6 and $z_1 \dots z_{12}$ in (3.14) and (3.15) are well defined if

$$q^{(1)} \neq 0, \quad q^{(1)} \neq \pm p^{(1)}, \quad q^{(1)} \neq \pm\sqrt{3}p^{(1)}. \quad (3.16)$$

As we are considering the case 1 with $|q^{(1)}/p^{(1)}| \geq 1$, $q^{(1)} = 0$ can be ignored for the case 1, which is also the reason that we choose the vertical transformation in the first transformation (i.e., the first arrow) in Fig. 4 for $|q^{(1)}/p^{(1)}| \geq 1$. So we discuss following 5 subcases of the case 1:

Subcase 1 of the case 1: $q^{(1)} \neq \pm p^{(1)}$ and $q^{(1)} \neq \pm\sqrt{3}p^{(1)}$. Recall that the Taylor series

$$\begin{array}{ccc}
\begin{array}{l} u^{(0,0)} u^{(1,0)} u^{(2,0)} u^{(3,0)} \\ u^{(0,1)} u^{(1,1)} u^{(2,1)} \\ u^{(0,2)} u^{(1,2)} \\ u^{(0,3)} \end{array} & \longrightarrow & \begin{array}{l} u^{(0,0)} u^{(1,0)} \\ u^{(0,1)} u^{(1,1)} \\ u^{(0,2)} u^{(1,2)} \\ u^{(0,3)} \end{array} & \longrightarrow & \begin{array}{l} u^{(1,0)} \\ u^{(1,1)} \\ u^{(1,2)} \end{array}
\end{array}$$

FIGURE 4. The illustration of vertical transformations for the subcase 1 with $q^{(1)} \neq \pm p^{(1)}$ and $q^{(1)} \neq \pm\sqrt{3}p^{(1)}$ of the case 1 with $|q^{(1)}/p^{(1)}| \geq 1$.

generates that

$$u(x + x_i^o, y + y_j^o) = \sum_{\substack{m,n=0 \\ m+n \leq 3}}^3 \frac{x^m y^n}{m!n!} u^{(m,n)} + \mathcal{O}(h^4) \quad \text{with } (x, y) \in (-2h, 2h)^2, \quad (3.17)$$

where $u^{(m,n)}$ is defined in (3.3) and (3.6). Plugging (3.11) and (3.13) into (3.17), we have

$$\begin{aligned}
u(x + x_i^o, y + y_j^o) &= \sum_{n=0}^2 G_{1,n}(x, y) u^{(1,n)} + \sum_{\substack{m,n=0 \\ m+n \leq 1}}^1 H_{m,n}(x, y) f^{(m,n)} \\
&\quad + \sum_{n=0}^3 V_n(x, y) g^{(n)} + \mathcal{O}(h^4) \quad \text{with } (x, y) \in (-2h, 2h)^2,
\end{aligned} \quad (3.18)$$

where

$$\begin{aligned}
G_{1,0}(x, y) &= x + \xi_1 y + \xi_2 y^2 + \xi_3 y^3 + \xi_4 x^2 + \xi_5 x^2 y + \xi_6 x^3, \\
G_{1,1}(x, y) &= \xi_7 y^2 + \xi_8 y^3 + \xi_9 x^2 + \xi_{10} x^2 y + \xi_{11} x^3 + xy, \\
G_{1,2}(x, y) &= \xi_{12} y^3 + \xi_{13} x^2 y - x^3/6 + xy^2/2, \\
H_{0,0}(x, y) &= \eta_1 y^2 + \eta_2 y^3 + \eta_3 x^2 + \eta_4 x^2 y + \eta_5 x^3, \\
H_{1,0}(x, y) &= \eta_8 y^3 + \eta_9 x^2 y + x^3/6, \quad H_{0,1}(x, y) = \eta_6 y^3 + \eta_7 x^2 y, \\
V_0(x, y) &= 1 + \omega_1 y^2 + \omega_2 y^3 + \omega_3 x^2 + \omega_4 x^2 y + \omega_5 x^3, \\
V_1(x, y) &= \omega_6 y + \omega_7 y^2 + \omega_8 y^3 + \omega_9 x^2 + \omega_{10} x^2 y + \omega_{11} x^3,
\end{aligned} \quad (3.19)$$

$$\begin{aligned}
V_2(x, y) &= \omega_{12}y^2 + \omega_{13}y^3 + \omega_{14}x^2 + \omega_{15}x^2y + \omega_{16}x^3, \\
V_3(x, y) &= \omega_{17}y^3 + \omega_{18}x^2y,
\end{aligned}$$

with

$$\begin{aligned}
\xi_1 &= s_1, & \xi_2 &= s_2/2, & \xi_3 &= s_4/6, & \xi_4 &= -(bs_1 + a + s_2)/2, \\
\xi_5 &= -[(d + b^{(0,1)})s_1 + s_2b + s_4 + a^{(0,1)}]/2, \\
\xi_6 &= (a^2 + (bs_1 + s_2)a - s_1b^{(1,0)} - a^{(1,0)} - d)/6, & \xi_7 &= s_3/2, \\
\xi_8 &= s_5/6, & \xi_9 &= -s_3/2, & \xi_{10} &= -(s_3b + a + s_5)/2, \\
\xi_{11} &= (s_3a - b)/6, & \xi_{12} &= s_6/6, & \xi_{13} &= -s_6/2, \\
\eta_1 &= -z_3/2, & \eta_2 &= -z_7/6, & \eta_3 &= (z_3 + 1)/2, \\
\eta_4 &= (z_3b + z_7)/2, & \eta_5 &= -(z_3 + 1)a/6, & \eta_6 &= -z_8/6, \\
\eta_7 &= (z_8 + 1)/2, & \eta_8 &= -z_{10}/6, & \eta_9 &= z_{10}/2, \\
\omega_1 &= -z_2/2, & \omega_2 &= -z_6/6, & \omega_3 &= (z_2 - d)/2, \\
\omega_4 &= (z_2b - d^{(0,1)} + z_6)/2, & \omega_5 &= [a(d - z_2) - d^{(1,0)}]/6, \\
\omega_6 &= -z_1, & \omega_7 &= -z_4/2, & \omega_8 &= -z_9/6, \\
\omega_9 &= (bz_1 + z_4)/2, & \omega_{10} &= [z_1(b^{(0,1)} + d) + z_4b + z_9]/2, \\
\omega_{11} &= [b^{(1,0)}z_1 - a(bz_1 + z_4)]/6, & \omega_{12} &= -z_5/2, \\
\omega_{13} &= -z_{11}/6, & \omega_{14} &= z_5/2, & \omega_{15} &= (z_5b + z_{11})/2, \\
\omega_{16} &= -z_5a/6, & \omega_{17} &= -z_{12}/6, & \omega_{18} &= z_{12}/2,
\end{aligned} \tag{3.20}$$

and s_1, \dots, s_6 and $z_1 \dots z_{12}$ are defined in (3.14) and (3.15), respectively. Let define

$$C_{r,\ell} := \sum_{\sigma=0}^3 c_{r,\ell,\sigma} h^\sigma, \quad \text{with } c_{r,\ell,\sigma} \text{ depending on } a, b, d \text{ in (1.3), and } c_{r,\ell,\sigma}|_{(x,y)=(x_i^o, y_j^o)} \in \mathbb{R}, \tag{3.21}$$

and assume that

$$\begin{aligned}
S &:= \{(r, \ell) : (x_i^o + rh, y_j^o + \ell h) \in \bar{\Omega} \text{ with } r, \ell = -1, 0, 1\}, \\
w &= (x_i - x_i^o)/h, & v &= (y_j - y_j^o)/h,
\end{aligned} \tag{3.22}$$

where $(x_i^o, y_j^o) \in \Omega$ is the orthogonal projection of the irregular stencil center point (x_i, y_j) (the set S consists of blue star and red points in Fig. 3). Next, we propose the derivation of the fourth-order compact FDM at the irregular stencil center point.

The algorithm to derive the fourth-order compact FDM at an irregular stencil center:
We define

$$\begin{aligned}
\mathcal{L}_h u_{i,j} &:= \sum_{\substack{r,\ell=-1 \\ (r,\ell) \in S}}^1 C_{r,\ell} \Big|_{(x,y)=(x_i^o, y_j^o)} u_{i+r, j+\ell} \\
&= \sum_{\substack{r,\ell=-1 \\ (r,\ell) \in S}}^1 C_{r,\ell} \Big|_{(x,y)=(x_i^o, y_j^o)} u(rh + wh + x_i^o, \ell h + vh + y_j^o),
\end{aligned} \tag{3.23}$$

where S, w, v are defined in (3.22). Applying (3.18) into (3.23), we obtain

$$\mathcal{L}_h u_{i,j} = \sum_{\substack{r,\ell=-1 \\ (r,\ell) \in S}}^1 C_{r,\ell} \Big|_{(x_i^o, y_j^o)} \sum_{n=0}^2 G_{1,n}([r+w]h, [\ell+v]h) u^{(1,n)}$$

$$\begin{aligned}
& + \sum_{\substack{r,\ell=-1 \\ (r,\ell) \in S}}^1 C_{r,\ell} \Big|_{(x_i^o, y_j^o)} \sum_{\substack{m,n=0 \\ m+n \leq 1}}^1 H_{m,n}([r+w]h, [\ell+v]h) f^{(m,n)} \\
& + \sum_{\substack{r,\ell=-1 \\ (r,\ell) \in S}}^1 C_{r,\ell} \Big|_{(x_i^o, y_j^o)} \sum_{n=0}^3 V_n([r+w]h, [\ell+v]h) g^{(n)} + \mathcal{O}(h^4).
\end{aligned} \tag{3.24}$$

Let

$$\mathcal{L}_h(u_h)_{i,j} := \sum_{\substack{r,\ell=-1 \\ (r,\ell) \in S}}^1 C_{r,\ell} \Big|_{(x,y)=(x_i^o, y_j^o)} (u_h)_{i,j} = F_{i,j}, \tag{3.25}$$

where

$$\begin{aligned}
F_{i,j} := \text{the terms of } & \left(\sum_{\substack{r,\ell=-1 \\ (r,\ell) \in S}}^1 C_{r,\ell} \Big|_{(x_i^o, y_j^o)} \sum_{\substack{m,n=0 \\ m+n \leq 1}}^1 H_{m,n}([r+w]h, [\ell+v]h) f^{(m,n)} \right. \\
& \left. + \sum_{\substack{r,\ell=-1 \\ (r,\ell) \in S}}^1 C_{r,\ell} \Big|_{(x_i^o, y_j^o)} \sum_{n=0}^3 V_n([r+w]h, [\ell+v]h) g^{(n)} \right) \\
& \text{with degree } \leq 3 \text{ in } h.
\end{aligned} \tag{3.26}$$

Then

$$\mathcal{L}_h(u - u_h)_{i,j} = \sum_{\substack{r,\ell=-1 \\ (r,\ell) \in S}}^1 C_{r,\ell} \Big|_{(x_i^o, y_j^o)} \sum_{n=0}^2 G_{1,n}([r+w]h, [\ell+v]h) u^{(1,n)} + \mathcal{O}(h^4). \tag{3.27}$$

To achieve the fourth-order consistency, we need to solve

$$\sum_{\substack{r,\ell=-1 \\ (r,\ell) \in S}}^1 C_{r,\ell} \Big|_{(x_i^o, y_j^o)} \sum_{n=0}^2 G_{1,n}([r+w]h, [\ell+v]h) u^{(1,n)} = \mathcal{O}(h^4). \tag{3.28}$$

By definitions of $C_{k,\ell}$ in (3.21) and $G_{1,n}(x, y)$ in (3.19), we have that (3.28) is equivalent to solve the following linear system

$$\sum_{\substack{r,\ell=-1 \\ (r,\ell) \in S}}^1 A_{r,\ell} c_{r,\ell} = 0, \quad c_{r,\ell} := \begin{bmatrix} c_{r,\ell,0} \\ c_{r,\ell,1} \\ c_{r,\ell,2} \\ c_{r,\ell,3} \end{bmatrix}, \tag{3.29}$$

with the 6×4 lower triangular matrix $A_{r,\ell}$

$$A_{r,\ell} := \begin{bmatrix} \tau_\ell \xi_1 + \mu_r & 0 & 0 & 0 \\ \mu_r^2 \xi_9 + \tau_\ell^2 \xi_7 + \mu_r \tau_\ell & 0 & 0 & 0 \\ \mu_r^2 \tau_\ell \xi_{13} + \tau_\ell^3 \xi_{12} - \mu_r^3/6 + \mu_r \tau_\ell^2/2 & 0 & 0 & 0 \\ \mu_r^2 \xi_4 + \tau_\ell^2 \xi_2 & \tau_\ell \xi_1 + \mu_r & 0 & 0 \\ \mu_r^3 \xi_{11} + \mu_r^2 \tau_\ell \xi_{10} + \tau_\ell^3 \xi_8 & \mu_r^2 \xi_9 + \tau_\ell^2 \xi_7 + \mu_r \tau_\ell & 0 & 0 \\ \mu_r^3 \xi_6 + \mu_r^2 \tau_\ell \xi_5 + \tau_\ell^3 \xi_3 & \mu_r^2 \xi_4 + \tau_\ell^2 \xi_2 & \tau_\ell \xi_1 + \mu_r & 0 \end{bmatrix}, \tag{3.30}$$

where

$$\mu_r = r + w, \quad \tau_\ell = \ell + v, \tag{3.31}$$

ξ_1, \dots, ξ_{13} are defined in (3.20), S, w and v are defined in (3.22), s_1, \dots, s_6 and $z_1 \dots z_{12}$ are defined in (3.14) and (3.15). From (3.30), the fourth column of $A_{r,\ell}$ is the zero vector, so we can set all $c_{r,\ell,3} = 0$

in (3.29). As we have at most 8 grid points in the stencil of the compact FDM at the irregular stencil center point, the matrix size of the linear system (3.29) is at most 6 by $(4 - 1)8 = 6$ by 24.

Substituting $C_{k,\ell}$ of (3.21), $H_{m,n}(x, y)$ and $V_n(x, y)$ of (3.19) into (3.26), we have that the explicit expression of $F_{i,j}$ in (3.26) is

$$\begin{aligned}
F_{i,j} = & \sum_{\substack{r,\ell=-1 \\ (r,\ell) \in S}}^1 \left\{ c_{r,\ell,0}g + \left\{ c_{r,\ell,0}g^{(1)}\omega_6\tau_\ell + c_{r,\ell,1}g \right\}h + \left\{ c_{r,\ell,0}[(\eta_1f + g\omega_1 + g^{(1)}\omega_7 \right. \right. \\
& + g^{(2)}\omega_{12})\tau_\ell^2 + \mu_r^2(\eta_3f + g\omega_3 + g^{(1)}\omega_9 + g^{(2)}\omega_{14})] + c_{r,\ell,1}g^{(1)}\omega_6\tau_\ell + c_{r,\ell,2}g \left. \right\}h^2 \\
& + \left\{ c_{r,\ell,0}[(\eta_2f + \eta_6f^{(0,1)} + \eta_8f^{(1,0)} + g\omega_2 + g^{(1)}\omega_8 + g^{(2)}\omega_{13} + g^{(3)}\omega_{17})\tau_\ell^3 \right. \\
& + \mu_r^2(\eta_4f + \eta_7f^{(0,1)} + \eta_9f^{(1,0)} + g\omega_4 + g^{(1)}\omega_{10} + g^{(2)}\omega_{15} + g^{(3)}\omega_{18})\tau_\ell \\
& + \mu_r^3(\eta_5f + \omega_5g + \omega_{11}g^{(1)} + \omega_{16}g^{(2)} + f^{(1,0)}/6)] + c_{r,\ell,1}(\eta_1f + g\omega_1 + g^{(1)}\omega_7 \\
& \left. \left. + g^{(2)}\omega_{12})\tau_\ell^2 + c_{r,\ell,2}g^{(1)}\omega_6\tau_\ell + c_{r,\ell,1}(\eta_3f + g\omega_3 + g^{(1)}\omega_9 + g^{(2)}\omega_{14})\mu_r^2 + c_{r,\ell,3}g \right\}h^3 \right\}, \tag{3.32}
\end{aligned}$$

μ_r and τ_ℓ are defined in (3.31), η_1, \dots, η_9 , and $\omega_1, \dots, \omega_{18}$ are defined in (3.20), S, w and v are defined in (3.22), s_1, \dots, s_6 and $z_1 \dots z_{12}$ are defined in (3.14) and (3.15), $g^{(1)}, g^{(2)}$, and $g^{(3)}$ are defined in (3.7).

Now, we can say that the compact FDM in (3.25) approximates the Dirichlet boundary condition $u = g$ at the point $(x_i^o, y_j^o) \in \partial\Omega$ with the fourth-order consistency, if $C_{r,\ell} = \sum_{\sigma=0}^3 c_{r,\ell,\sigma}h^\sigma$ and $F_{i,j}$ in (3.32) are obtained by solving (3.29) with (3.30) and satisfying $c_{0,0,0} \neq 0$ and $F_{i,j}|_{h=0} = g$. Using (3.32), $F_{i,j}|_{h=0} = g$ if and only if $\sum_{\substack{r,\ell=-1 \\ (r,\ell) \in S}}^1 c_{r,\ell,0} = 1$.

In summary, we propose the fourth-order compact FDM to solve (1.1) at the irregular stencil center point for the subcase 1 of the case 1 as follows:

Theorem 3.1. *Let $\alpha > 0, \vec{\beta}, \kappa, \phi, u$ be smooth in $\bar{\Omega}$ in (1.1), $\partial\Omega$ be a smooth boundary curve, functions a, b, d, f be defined in (1.2), and $(x_i^o, y_j^o) \in \Omega$ be the orthogonal projection of the irregular stencil center point (x_i, y_j) . If*

$$(x_i^o, y_j^o) = (p(t_k^o), q(t_k^o)), \quad |q'(t_k^o)/p'(t_k^o)| \geq 1, \quad q'(t_k^o) \neq \pm p'(t_k^o), \quad q'(t_k^o) \neq \pm\sqrt{3}p'(t_k^o).$$

Then the following compact FDM (see Fig. 3 for illustrations)

$$\mathcal{L}_h(u_h)_{i,j} := \sum_{\substack{r,\ell=-1 \\ (r,\ell) \in S}}^1 C_{r,\ell} \Big|_{(x,y)=(x_i^o,y_j^o)} (u_h)_{i+r,j+\ell} = F_{i,j} \Big|_{(x,y)=(x_i^o,y_j^o)},$$

achieves the fourth-order consistency for the Dirichlet boundary condition $u = g$ at the point $(x_i^o, y_j^o) \in \partial\Omega$, where S is defined in (3.22), the right-hand side $F_{i,j}$ of the stencil is defined in (3.32), the left-hand side $C_{r,\ell} = \sum_{\sigma=0}^3 c_{r,\ell,\sigma}h^\sigma$ of the stencil is obtained by solving (3.29) with (3.30), $c_{0,0,0} \neq 0$, and $\sum_{\substack{r,\ell=-1 \\ (r,\ell) \in S}}^1 c_{r,\ell,0} = 1$.

Remark 3.1. *From (3.11) and (3.13)–(3.15), we observe that first-order derivatives of $\alpha, \vec{\beta}, \kappa, \phi$ in (1.1) and up to third-order derivatives of the Dirichlet boundary function g and the parametric equation $(p(t), q(t))$ in (3.1) are sufficient to construct the fourth-order compact FDM at the irregular stencil center point.*

Remark 3.2. *Note that the solution $c_{r,\ell}$ in (3.29) is not unique. In our numerical examples, we set $c_{0,0,0} = 1$ and use the MATLAB function 'mldivide' to solve (3.29) to set the remaining free parameters to zero automatically.*

Remark 3.3. *We still need to derive FDMs for the remaining 4 subcases for the case 1. Readers can choose other $(\tilde{x}_i^o, \tilde{y}_j^o) \in \partial\Omega$ that is near (x_i^o, y_j^o) to replace (x_i^o, y_j^o) to avoid the remaining 4 subcases.*

Then readers can utilize the FDM of the subcase 1 to completely handle any irregular stencil center points in the case 1. In our numerical examples, each of (x_i^o, y_j^o) is the orthogonal projection of the irregular stencil center point (x_i, y_j) , so we employ fourth-order compact FDMs in 5 subcases for the case 1 to verify the accuracy and the convergence rate. As the remaining 4 subcases only appear when $q^{(1)} = \pm p^{(1)}$ and $q^{(1)} = \pm\sqrt{3}p^{(1)}$, for the sake of brevity, we only provide Fig. 5–Fig. 7 which are sufficient for readers to obtain corresponding fourth-order compact FDMs by similarly applying (3.8)–(3.32) in the subcase 1.

Remark 3.4. Note that transformations in Fig. 4–Fig. 7 are not unique. The first transformation in Fig. 4–Fig. 7 is the vertical transformation to avoid the subcase $q^{(1)} = 0$ to make implementation easy. While second transformations are different to avoid the zero denominator in the stencil of the proposed FDM. In future we plan to establish the optimal transformation to reduce the pollution effect to achieve the smallest error by adopting the truncation error minimization strategy in [12, 15].

$$\begin{array}{ccc}
 u^{(0,0)} u^{(1,0)} u^{(2,0)} u^{(3,0)} & & u^{(0,0)} u^{(1,0)} & & u^{(1,0)} \\
 u^{(0,1)} u^{(1,1)} u^{(2,1)} & \longrightarrow & u^{(0,1)} u^{(1,1)} & & u^{(0,2)} \\
 u^{(0,2)} u^{(1,2)} & & u^{(0,2)} u^{(1,2)} & \longrightarrow & u^{(1,2)} \\
 u^{(0,3)} & & u^{(0,3)} & &
 \end{array}$$

FIGURE 5. The illustration of vertical transformations for the subcase 2 with $q^{(1)} = p^{(1)}$ of the case 1 with $|q^{(1)}/p^{(1)}| \geq 1$.

$$\begin{array}{ccc}
 u^{(0,0)} u^{(1,0)} u^{(2,0)} u^{(3,0)} & & u^{(0,0)} u^{(1,0)} & & u^{(0,1)} \\
 u^{(0,1)} u^{(1,1)} u^{(2,1)} & \longrightarrow & u^{(0,1)} u^{(1,1)} & & u^{(0,2)} \\
 u^{(0,2)} u^{(1,2)} & & u^{(0,2)} u^{(1,2)} & \longrightarrow & u^{(1,2)} \\
 u^{(0,3)} & & u^{(0,3)} & &
 \end{array}$$

FIGURE 6. The illustration of vertical transformations for the subcase 3 with $q^{(1)} = -p^{(1)}$ of the case 1 with $|q^{(1)}/p^{(1)}| \geq 1$.

$$\begin{array}{ccc}
 u^{(0,0)} u^{(1,0)} u^{(2,0)} u^{(3,0)} & & u^{(0,0)} u^{(1,0)} & & u^{(0,1)} \\
 u^{(0,1)} u^{(1,1)} u^{(2,1)} & \longrightarrow & u^{(0,1)} u^{(1,1)} & & u^{(1,1)} \\
 u^{(0,2)} u^{(1,2)} & & u^{(0,2)} u^{(1,2)} & \longrightarrow & u^{(0,3)} \\
 u^{(0,3)} & & u^{(0,3)} & &
 \end{array}$$

FIGURE 7. The illustration of vertical transformations for subcases 4 and 5 with $q^{(1)} = \pm\sqrt{3}p^{(1)}$ of the case 1 with $|q^{(1)}/p^{(1)}| \geq 1$.

Next, we construct the fourth-order compact FDM at the irregular stencil center point for the case 2 with $|q^{(1)}/p^{(1)}| \leq 1$.

Case 2: $|q^{(1)}/p^{(1)}| \leq 1$. Similar to the case 1, we also need to discuss 5 subcases.

Subcase 1 of the case 2: $q^{(1)} \neq \pm p^{(1)}$ and $q^{(1)} \neq \pm\frac{\sqrt{3}}{3}p^{(1)}$. We present the fourth-order compact FDM in the following Theorem 3.2 directly, while Theorem 3.2 can be obtained by repeating (3.8)–(3.32) with using transformations in Fig. 8.

Theorem 3.2. Let $\alpha > 0, \vec{\beta}, \kappa, \phi, u$ be smooth in $\bar{\Omega}$ in (1.1), $\partial\Omega$ be a smooth boundary curve, functions a, b, d, f be defined in (1.2), and $(x_i^o, y_j^o) \in \Omega$ be the orthogonal projection of the irregular stencil center point (x_i, y_j) . If

$$(x_i^o, y_j^o) = (p(t_k^o), q(t_k^o)), \quad |q'(t_k^o)/p'(t_k^o)| \leq 1, \quad q'(t_k^o) \neq \pm p'(t_k^o), \quad q'(t_k^o) \neq \pm\frac{\sqrt{3}}{3}p'(t_k^o).$$

$$\begin{array}{ccc}
\begin{array}{l} u^{(0,0)} u^{(1,0)} u^{(2,0)} u^{(3,0)} \\ u^{(0,1)} u^{(1,1)} u^{(2,1)} \\ u^{(0,2)} u^{(1,2)} \\ u^{(0,3)} \end{array} & \longrightarrow & \begin{array}{l} u^{(0,0)} u^{(0,1)} \\ u^{(1,0)} u^{(1,1)} \\ u^{(2,0)} u^{(2,1)} \\ u^{(3,0)} \end{array} \longrightarrow \begin{array}{l} u^{(0,1)} \\ u^{(1,1)} \\ u^{(2,1)} \end{array}
\end{array}$$

FIGURE 8. The illustration of horizontal transformations for the subcase 1 with $q^{(1)} \neq \pm p^{(1)}$ and $q^{(1)} \neq \pm \frac{\sqrt{3}}{3} p^{(1)}$ of the case 2 with $|q^{(1)}/p^{(1)}| \leq 1$.

Then the following compact FDM (see Fig. 3 for illustrations)

$$\mathcal{L}_h(u_h)_{i,j} := \sum_{\substack{r,\ell=-1 \\ (r,\ell) \in S}}^1 C_{r,\ell} \Big|_{(x,y)=(x_i^o, y_j^o)} (u_h)_{i+r, j+\ell} = F_{i,j} \Big|_{(x,y)=(x_i^o, y_j^o)},$$

achieves the fourth-order consistency for the Dirichlet boundary condition $u = g$ at the point $(x_i^o, y_j^o) \in \partial\Omega$, where the left-hand side $C_{r,\ell} = \sum_{\sigma=0}^3 c_{r,\ell,\sigma} h^\sigma$ of the stencil is obtained by solving

$$\sum_{\substack{r,\ell=-1 \\ (r,\ell) \in S}}^1 A_{r,\ell} c_{r,\ell} = 0, \quad c_{r,\ell} := \begin{bmatrix} c_{r,\ell,0} \\ c_{r,\ell,1} \\ c_{r,\ell,2} \\ c_{r,\ell,3} \end{bmatrix},$$

with the 6×4 lower triangular matrix $A_{r,\ell}$

$$A_{r,\ell} := \begin{bmatrix} \mu_r \xi_3 + \tau_\ell & 0 & 0 & 0 \\ \mu_r^2 \xi_{10} + \tau_\ell^2 \xi_7 + \mu_r \tau_\ell & 0 & 0 & 0 \\ \mu_r \xi_{12} \tau_\ell^2 - \tau_\ell^3/6 + \mu_r^2 \tau_\ell/2 + \mu_r^3 \xi_{13} & 0 & 0 & 0 \\ \mu_r^2 \xi_5 + \tau_\ell^2 \xi_1 & \mu_r \xi_3 + \tau_\ell & 0 & 0 \\ \mu_r^3 \xi_{11} + \mu_r \tau_\ell^2 \xi_9 + \tau_\ell^3 \xi_8 & \mu_r^2 \xi_{10} + \tau_\ell^2 \xi_7 + \mu_r \tau_\ell & 0 & 0 \\ \mu_r^3 \xi_6 + \mu_r \tau_\ell^2 \xi_4 + \tau_\ell^3 \xi_2 & \mu_r^2 \xi_5 + \tau_\ell^2 \xi_1 & \mu_r \xi_3 + \tau_\ell & 0 \end{bmatrix},$$

$$c_{0,0,0} \neq 0, \quad \sum_{\substack{r,\ell=-1 \\ (r,\ell) \in S}}^1 c_{r,\ell,0} = 1,$$

the right-hand side $F_{i,j}$ of the stencil is defined as

$$\begin{aligned}
F_{i,j} = \sum_{\substack{r,\ell=-1 \\ (r,\ell) \in S}}^1 & \left\{ g c_{r,\ell,0} + \left\{ c_{r,\ell,0} g^{(1)} \mu_r \omega_8 + c_{r,\ell,1} g \right\} h + \left\{ g c_{r,\ell,2} + g^{(1)} \omega_8 \mu_r c_{r,\ell,1} + ([\eta_4 f + g \omega_4 \right. \right. \\
& + g^{(1)} \omega_{10} + g^{(2)} \omega_{15}] \mu_r^2 + \tau_\ell^2 [\eta_1 f + g \omega_1 + g^{(1)} \omega_6 + g^{(2)} \omega_{12}] c_{r,\ell,0} \left. \right\} h^2 + \left\{ ([\eta_5 f + \eta_7 f^{(0,1)} \right. \\
& + \eta_9 f^{(1,0)} + g \omega_5 + g^{(1)} \omega_{11} + g^{(2)} \omega_{16} + g^{(3)} \omega_{18}] \mu_r^3 + \tau_\ell^2 (\eta_3 f + \eta_6 f^{(0,1)} + \eta_8 f^{(1,0)} + g \omega_3 \\
& + g^{(1)} \omega_9 + g^{(2)} \omega_{14} + g^{(3)} \omega_{17}) \mu_r + \tau_\ell^3 [g \omega_2 + g^{(1)} \omega_7 + g^{(2)} \omega_{13} + f \eta_2 + f^{(0,1)}/6] c_{r,\ell,0} \\
& + c_{r,\ell,1} (\eta_4 f + g \omega_4 + g^{(1)} \omega_{10} + g^{(2)} \omega_{15}) \mu_r^2 + g^{(1)} \omega_8 \mu_r c_{r,\ell,2} + c_{r,\ell,1} (\eta_1 f + g \omega_1 + g^{(1)} \omega_6 \\
& \left. \left. + g^{(2)} \omega_{12}) \tau_\ell^2 + g c_{r,\ell,3} \right\} h^3 \right\},
\end{aligned}$$

where

$$S := \{(r, \ell) : (x_i^o + rh, y_j^o + \ell h) \in \bar{\Omega} \text{ with } r, \ell = -1, 0, 1\},$$

$$w = (x_i - x_i^o)/h, \quad v = (y_j - y_j^o)/h, \quad \mu_r = r + w, \quad \tau_\ell = \ell + v,$$

$$\xi_1 = -(as_1 + b + s_2)/2,$$

$$\xi_2 = (b^2 + (as_1 + s_2)b - s_1 a^{(0,1)} - b^{(0,1)} - d)/6,$$

$$\begin{aligned}
\xi_3 &= s_1, & \xi_4 &= (s_1(-d - a^{(1,0)}) - s_2a - s_4 - b^{(1,0)})/2, \\
\xi_5 &= s_2/2, & \xi_6 &= s_4/6, & \xi_7 &= -s_3/2, & \xi_8 &= (s_3b - a)/6, \\
\xi_9 &= -(s_3a + b + s_5)/2, & \xi_{10} &= s_3/2, & \xi_{11} &= s_5/6, \\
\xi_{12} &= -s_6/2, & \xi_{13} &= s_6/6, \\
\eta_1 &= (z_3 + 1)/2, & \eta_2 &= -(z_3 + 1)b/6, & \eta_3 &= (z_3a + z_7)/2, \\
\eta_4 &= -z_3/2, & \eta_5 &= -z_7/6, & \eta_6 &= z_8/2, & \eta_7 &= -z_8/6, \\
\eta_8 &= (z_{10} + 1)/2, & \eta_9 &= -z_{10}/6, \\
\omega_1 &= (z_2 - d)/2, & \omega_2 &= ([-z_2 + d]b - d^{(0,1)})/6, \\
\omega_3 &= (z_2a - d^{(1,0)} + z_6)/2, & \omega_4 &= -z_2/2, & \omega_5 &= -z_6/6, \\
\omega_6 &= (az_1 + z_4)/2, & \omega_7 &= (a^{(0,1)}z_1 - [az_1 + z_4]b)/6, \\
\omega_8 &= -z_1, & \omega_9 &= ([a^{(1,0)} + d]z_1 + z_4a + z_9)/2, \\
\omega_{10} &= -z_4/2, & \omega_{11} &= -z_9/6, & \omega_{12} &= z_5/2, \\
\omega_{13} &= -z_5b/6, & \omega_{14} &= (z_5a + z_{11})/2, & \omega_{15} &= -z_5/2, \\
\omega_{16} &= -z_{11}/6, & \omega_{17} &= z_{12}/2, & \omega_{18} &= -z_{12}/6,
\end{aligned}$$

with

$$\begin{aligned}
s_1 &= -q^{(1)}/p^{(1)}, \\
s_2 &= \{(b[q^{(1)}]^2 - q^{(2)})p^{(1)} - a[q^{(1)}]^3 \\
&\quad + p^{(2)}q^{(1)}\} / \{p^{(1)}([p^{(1)}]^2 - [q^{(1)}]^2)\}, \\
s_3 &= -2p^{(1)}q^{(1)} / \{[p^{(1)}]^2 - [q^{(1)}]^2\}, \\
s_4 &= \{a^{(0,1)}[q^{(1)}]^6 - 3(a^2 - a^{(1,0)} + b^{(0,1)}/3 - 2d/3)p^{(1)}[q^{(1)}]^5 \\
&\quad + ([p^{(1)}]^2(4ab - a^{(0,1)} - 3b^{(1,0)}) - bp^{(2)}[q^{(1)}]^4 + ([p^{(1)}]^3(b^{(0,1)} \\
&\quad - b^2 - 3a^{(1,0)} - 2d) + (6ap^{(2)} + bq^{(2)})p^{(1)} - p^{(3)})[q^{(1)}]^3 \\
&\quad + (3b^{(1,0)}[p^{(1)}]^4 - 3(2aq^{(2)} + bp^{(2)})[p^{(1)}]^2 + p^{(1)}q^{(3)} \\
&\quad + 3p^{(2)}q^{(2)})[q^{(1)}]^2 + 3p^{(1)}(b[p^{(1)}]^2q^{(2)} + p^{(1)}p^{(3)}/3 \\
&\quad - [p^{(2)}]^2 - [q^{(2)}]^2)q^{(1)} - [p^{(1)}]^3q^{(3)} + 3[p^{(1)}]^2p^{(2)}q^{(2)}\} \\
&\quad / \{[p^{(1)}]^2([p^{(1)}]^4 - 4[p^{(1)}]^2[q^{(1)}]^2 + 3[q^{(1)}]^4)\}, \\
s_5 &= \{3b[p^{(1)}]^3[q^{(1)}]^2 - 5a[p^{(1)}]^2[q^{(1)}]^3 - a[q^{(1)}]^5 - bp^{(1)}[q^{(1)}]^4 \\
&\quad - 3[p^{(1)}]^3q^{(2)} + 3[p^{(1)}]^2p^{(2)}q^{(1)} - 3p^{(1)}[q^{(1)}]^2q^{(2)} + 3p^{(2)}[q^{(1)}]^3\} \\
&\quad / \{p^{(1)}([p^{(1)}]^4 - 4[p^{(1)}]^2[q^{(1)}]^2 + 3[q^{(1)}]^4)\}, \\
s_6 &= \{[q^{(1)}]^3 - 3[p^{(1)}]^2q^{(1)}\} / \{p^{(1)}([p^{(1)}]^2 - 3[q^{(1)}]^2)\},
\end{aligned}$$

and

$$\begin{aligned}
z_1 &= -1/p^{(1)}, \\
z_2 &= -d[q^{(1)}]^2 / \{[p^{(1)}]^2 - [q^{(1)}]^2\}, \\
z_3 &= [q^{(1)}]^2 / \{[p^{(1)}]^2 - [q^{(1)}]^2\}, \\
z_4 &= \{-a[q^{(1)}]^2 + p^{(2)}\} / \{p^{(1)}([p^{(1)}]^2 - [q^{(1)}]^2)\}, \\
z_5 &= -1 / \{[p^{(1)}]^2 - [q^{(1)}]^2\}, \\
z_6 &= -q^{(1)} \{3adp^{(1)}[q^{(1)}]^3 - bd[p^{(1)}]^2[q^{(1)}]^2\}
\end{aligned}$$

$$\begin{aligned}
& + d^{(0,1)}[p^{(1)}]^2[q^{(1)}]^2 - d^{(0,1)}[q^{(1)}]^4 + 3d^{(1,0)}[p^{(1)}]^3q^{(1)} \\
& - 3d^{(1,0)}p^{(1)}[q^{(1)}]^3 + 3d[p^{(1)}]^2q^{(2)} - 3dp^{(1)}p^{(2)}q^{(1)} \} \\
& / \{ p^{(1)}([p^{(1)}]^4 - 4[p^{(1)}]^2[q^{(1)}]^2 + 3[q^{(1)}]^4) \}, \\
z_7 &= 3q^{(1)} \{ a[q^{(1)}]^3 - bp^{(1)}[q^{(1)}]^2/3 + p^{(1)}q^{(2)} - p^{(2)}q^{(1)} \} \\
& / \{ [p^{(1)}]^4 - 4[p^{(1)}]^2[q^{(1)}]^2 + 3[q^{(1)}]^4 \}, \\
z_8 &= [q^{(1)}]^3 / \{ p^{(1)}([p^{(1)}]^2 - 3[q^{(1)}]^2) \}, \\
z_9 &= \{ a^{(0,1)}[q^{(1)}]^5 - 3p^{(1)}(a^2 - a^{(1,0)} - d)[q^{(1)}]^4 \\
& + ((ab - a^{(0,1)})[p^{(1)}]^2 - bp^{(2)})[q^{(1)}]^3 + (-3(a^{(1,0)} \\
& + d)[p^{(1)}]^3 + 6ap^{(1)}p^{(2)} - p^{(3)})[q^{(1)}]^2 - 3q^{(2)}(a[p^{(1)}]^2 \\
& - p^{(2)})q^{(1)} + [p^{(1)}]^2p^{(3)} - 3p^{(1)}[p^{(2)}]^2 \} / \{ [p^{(1)}]^2([p^{(1)}]^4 \\
& - 4[p^{(1)}]^2[q^{(1)}]^2 + 3[q^{(1)}]^4) \}, \\
z_{10} &= 3[q^{(1)}]^2 / \{ [p^{(1)}]^2 - 3[q^{(1)}]^2 \}, \\
z_{11} &= \{ b[q^{(1)}]^3 - 3ap^{(1)}[q^{(1)}]^2 + 3p^{(1)}p^{(2)} - 3q^{(1)}q^{(2)} \} \\
& / \{ p^{(1)}([p^{(1)}]^4 - 4[p^{(1)}]^2[q^{(1)}]^2 + 3[q^{(1)}]^4) \}, \\
z_{12} &= -1 / \{ p^{(1)}([p^{(1)}]^2 - 3[q^{(1)}]^2) \}.
\end{aligned}$$

Similar to subcases 2 to 5 of the case 1, we also provide Fig. 9–Fig. 11 for subcases 2 to 5 of the case 2 which are sufficient to derive corresponding fourth-order compact FDMs at irregular stencil center points in the remaining 4 subcases by adopting (3.8)–(3.32) similarly.

$$\begin{array}{ccc}
\begin{array}{l} u^{(0,0)} u^{(1,0)} u^{(2,0)} u^{(3,0)} \\ u^{(0,1)} u^{(1,1)} u^{(2,1)} \\ u^{(0,2)} u^{(1,2)} \\ u^{(0,3)} \end{array} & \longrightarrow & \begin{array}{l} u^{(0,0)} u^{(0,1)} \\ u^{(1,0)} u^{(1,1)} \\ u^{(2,0)} u^{(2,1)} \\ u^{(3,0)} \end{array} & \longrightarrow & \begin{array}{l} u^{(1,0)} \\ u^{(2,0)} \\ u^{(3,0)} \end{array}
\end{array}$$

FIGURE 9. The illustration of horizontal transformations for the subcase 2 with $q^{(1)} = p^{(1)}$ of the case 2 with $|q^{(1)}/p^{(1)}| \leq 1$.

$$\begin{array}{ccc}
\begin{array}{l} u^{(0,0)} u^{(1,0)} u^{(2,0)} u^{(3,0)} \\ u^{(0,1)} u^{(1,1)} u^{(2,1)} \\ u^{(0,2)} u^{(1,2)} \\ u^{(0,3)} \end{array} & \longrightarrow & \begin{array}{l} u^{(0,0)} u^{(0,1)} \\ u^{(1,0)} u^{(1,1)} \\ u^{(2,0)} u^{(2,1)} \\ u^{(3,0)} \end{array} & \longrightarrow & \begin{array}{l} u^{(0,1)} \\ u^{(2,0)} \\ u^{(3,0)} \end{array}
\end{array}$$

FIGURE 10. The illustration of horizontal transformations for the subcase 3 with $q^{(1)} = -p^{(1)}$ of the case 2 with $|q^{(1)}/p^{(1)}| \leq 1$.

$$\begin{array}{ccc}
\begin{array}{l} u^{(0,0)} u^{(1,0)} u^{(2,0)} u^{(3,0)} \\ u^{(0,1)} u^{(1,1)} u^{(2,1)} \\ u^{(0,2)} u^{(1,2)} \\ u^{(0,3)} \end{array} & \longrightarrow & \begin{array}{l} u^{(0,0)} u^{(0,1)} \\ u^{(1,0)} u^{(1,1)} \\ u^{(2,0)} u^{(2,1)} \\ u^{(3,0)} \end{array} & \longrightarrow & \begin{array}{l} u^{(0,1)} \\ u^{(1,1)} \\ u^{(3,0)} \end{array}
\end{array}$$

FIGURE 11. The illustration of horizontal transformations for subcases 4 and 5 with $q^{(1)} = \pm \frac{\sqrt{3}}{3}p^{(1)}$ of the case 2 with $|q^{(1)}/p^{(1)}| \leq 1$.

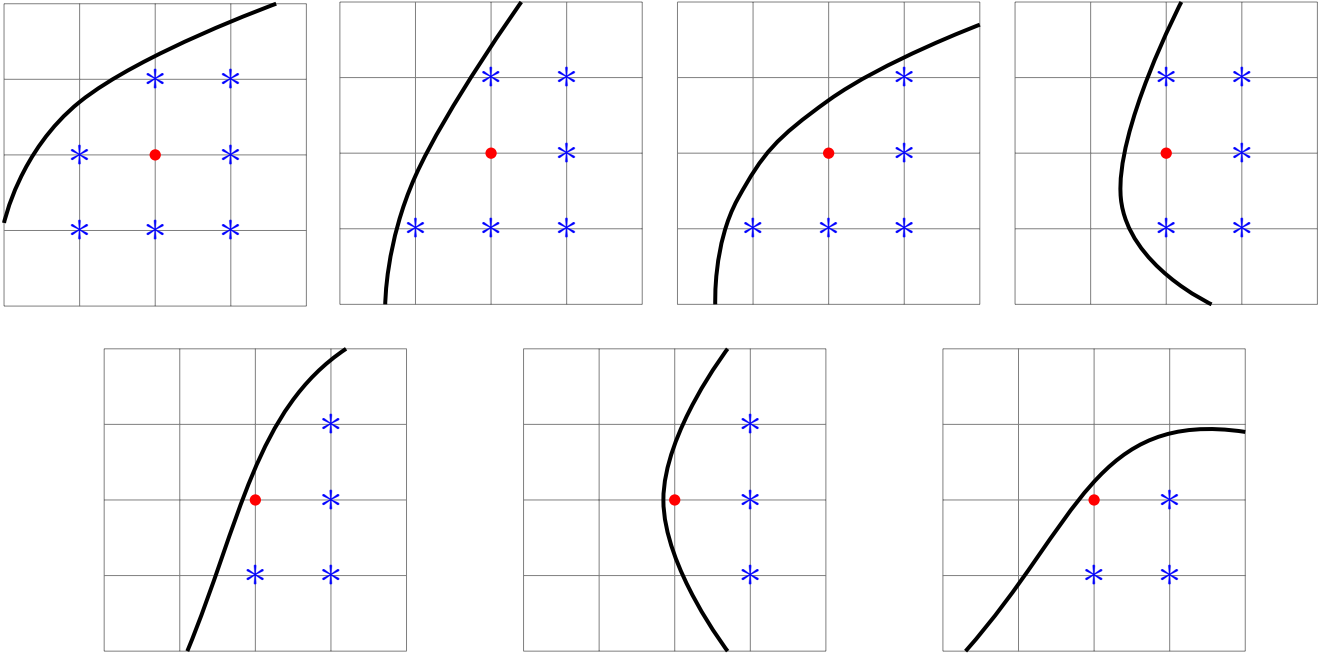


FIGURE 12. Up to symmetric transformations and rotations, compact FDMs at irregular stencil center points only have the above 7 configurations for any complex boundary curves when the mesh size h is reasonably small, where red points are irregular stencil center points, blue star points are remaining grid points used in compact FDMs, and black curves are boundaries. See [13, Figs. 3-5] for more configurations if h is not sufficiently small.

4. NUMERICAL EXPERIMENTS

Recall that we define that $u_{i,j} = u(x_i, y_j)$, and $(u_h)_{i,j}$ = the value of u_h at the grid point (x_i, y_j) , where Ω is discretized by the following uniform Cartesian grid:

$$\bar{\Omega}_h := \{(x_i, y_j) \cap \bar{\Omega} \quad : \quad (x_i, y_j) := (ih, jh), \quad i, j = 0, \pm 1, \pm 2, \dots, \quad \text{and} \quad h := 1/N, \quad N \in \mathbb{N}\}.$$

Then we define the following l_2 and l_∞ norms of errors to verify the convergence rate of the proposed fourth-order compact FDM

$$\frac{\|u_h - u\|_2}{\|u\|_2} := \sqrt{\frac{\sum_{(x_i, y_j) \in \bar{\Omega}_h} |(u_h)_{i,j} - u(x_i, y_j)|^2}{\sum_{(x_i, y_j) \in \bar{\Omega}_h} |u(x_i, y_j)|^2}},$$

$$\|u_h - u\|_\infty := \max_{(x_i, y_j) \in \bar{\Omega}_h} |(u_h)_{i,j} - u(x_i, y_j)|.$$

In the following Examples 4.1 to 4.3, the domain Ω is very thin and/or the boundary curve $\partial\Omega$ is sharply varying and/or exhibits the high frequency.

Example 4.1. The functions of the convection-diffusion-reaction equation (1.1) on a curved domain Ω are given by

$$\begin{aligned} u &= \sin(6x) \cos(6y), & \alpha &= \exp(x + y), \\ \beta_1 &= \exp(x - y), & \beta_2 &= \cos(x) \cos(y), & \kappa &= \exp(x + y), \\ \Omega &= \{(x(t), y(t)) : x(t)^2 + y(t)^2 < [0.3 + 0.2 \sin(20t)]^2, \quad t \in [0, 2\pi)\}, \end{aligned}$$

the source term ϕ and the Dirichlet boundary function g are obtained by plugging above functions into (1.1). The numerical results are presented in Table 1 and Fig. 13.

Remark 4.1. Up to symmetric transformations and rotations, the stencil of the proposed fourth-order compact FDM at the irregular stencil center point only has 7 configurations depicted in Fig. 12 for any complicated boundary curves, when the mesh size h is reasonably small. So we notice that

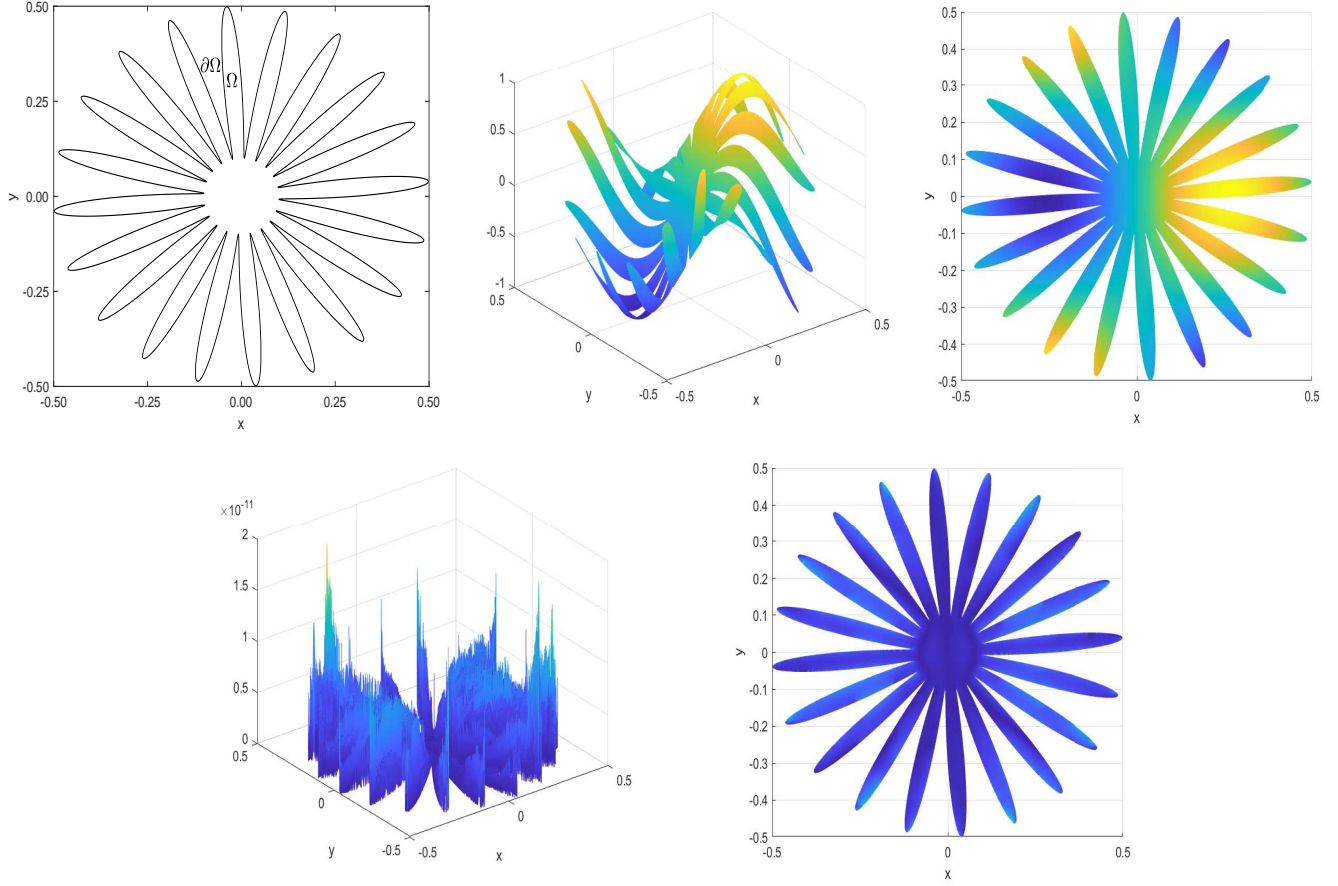


FIGURE 13. Performance in Example 4.1 of the proposed fourth-order compact FDM. The domain Ω that is enclosed by a 20-leaf boundary curve $\partial\Omega$ (left panel in the first row), u_h on $\bar{\Omega}_h$ with $h = 1/2^{12}$ (middle and right panels in the first row), and $|u_h - u|$ on $\bar{\Omega}_h$ with $h = 1/2^{12}$ (left and right panels in the second row).

TABLE 1. Performance in Example 4.1 of the proposed fourth-order compact FDM.

h	$\frac{\ u_h - u\ _2}{\ u\ _2}$	order	$\ u_h - u\ _\infty$	order
$1/2^5$	9.0345E-01		4.4766E+00	
$1/2^6$	5.4344E-02	4.06	5.9199E-01	2.92
$1/2^7$	6.8879E-04	6.30	3.9511E-03	7.23
$1/2^8$	3.5861E-07	10.91	2.2467E-06	10.78
$1/2^9$	2.2640E-08	3.99	8.0102E-08	4.81
$1/2^{10}$	1.3953E-09	4.02	5.1896E-09	3.95
$1/2^{11}$	8.7934E-11	3.99	3.3360E-10	3.96
$1/2^{12}$	4.8243E-12	4.19	1.9917E-11	4.07

the convergence rate increases to 11 when $h = 1/2^8$, and then the convergence rate is stabilized at 4 when $h < 1/2^8$ (the reasonably fine meshes) in Table 1 for Example 4.1. Similar observations can be found in Tables 2 and 3 for Example 4.2 and Tables 4 to 7 for Example 4.3.

Example 4.2. The functions of the convection-diffusion-reaction equation (1.1) on a curved domain Ω are given by

$$u = \cos(k(x - y)), \quad k = 5, 10, \quad \alpha = 4 + \sin(4x) \cos(4y),$$

$$\beta_1 = \sin(x + 2y), \quad \beta_2 = \cos(2x) \cos(3y), \quad \kappa = \cos(3x + y),$$

$$\Omega = \{(x(t), y(t)) : [0.2 + 0.15 \sin(5t)]^2 < x(t)^2 + y(t)^2 < [0.3 + 0.16 \sin(5t)]^2, \quad t \in [0, 2\pi)\},$$

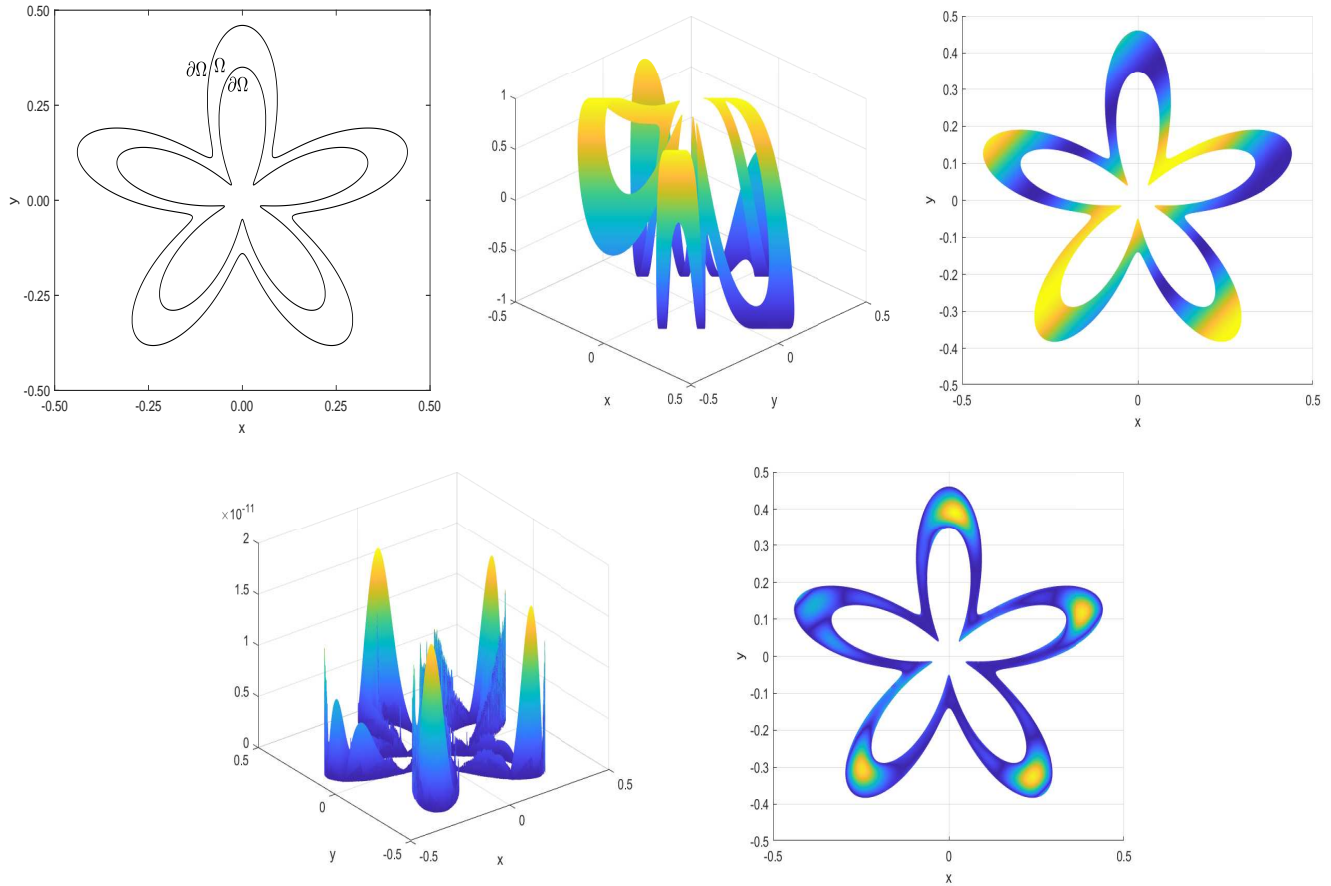


FIGURE 14. Performance in Example 4.2 of the proposed fourth-order compact FDM with $u = \cos(10(x - y))$. The domain $\Omega = \{(x(t), y(t)) : [0.2 + 0.15 \sin(5t)]^2 < x(t)^2 + y(t)^2 < [0.3 + 0.16 \sin(5t)]^2, t \in [0, 2\pi]\}$ that is enclosed by two 5-leaf boundary curves $\partial\Omega$ (left panel in the first row), u_h on $\bar{\Omega}_h$ with $h = 1/2^{13}$ (middle and right panels in the first row), and $|u_h - u|$ on $\bar{\Omega}_h$ with $h = 1/2^{13}$ (left and right panels in the second row).

$$\Omega = \{(x(t), y(t)) : [0.1 + 0.05 \sin(5t)]^2 < x(t)^2 + y(t)^2 < [0.35 + 0.1 \sin(20t)]^2, t \in [0, 2\pi]\},$$

the source term ϕ and the Dirichlet boundary function g are obtained by plugging above functions into (1.1). The numerical results are presented in Tables 2 and 3 and Figs. 14 and 15.

TABLE 2. Performance in Example 4.2 of the proposed fourth-order compact FDM, where $u = \cos(10(x - y))$ and $\Omega = \{(x(t), y(t)) : [0.2 + 0.15 \sin(5t)]^2 < x(t)^2 + y(t)^2 < [0.3 + 0.16 \sin(5t)]^2, t \in [0, 2\pi]\}$.

h	$\frac{\ u_h - u\ _2}{\ u\ _2}$	order	$\ u_h - u\ _\infty$	order
$1/2^8$	2.7119E-04		1.1166E-02	
$1/2^9$	2.2578E-07	10.23	3.6442E-06	11.58
$1/2^{10}$	1.3317E-08	4.08	1.9743E-07	4.21
$1/2^{11}$	8.3414E-10	4.00	3.4156E-09	5.85
$1/2^{12}$	5.2193E-11	4.00	2.2667E-10	3.91
$1/2^{13}$	7.9523E-12	2.71	1.6872E-11	3.75

Example 4.3. The functions of the convection-diffusion-reaction equation (1.1) on a curved domain Ω are given by

$$\begin{aligned} u &= \sin(kx) \cos(ky), & k &= 4, 10, 50, & \alpha &= \exp(x + y), \\ \beta_1 &= \exp(x - y), & \beta_2 &= \cos(x) \cos(y), & \kappa &= \exp(x + y), \end{aligned}$$

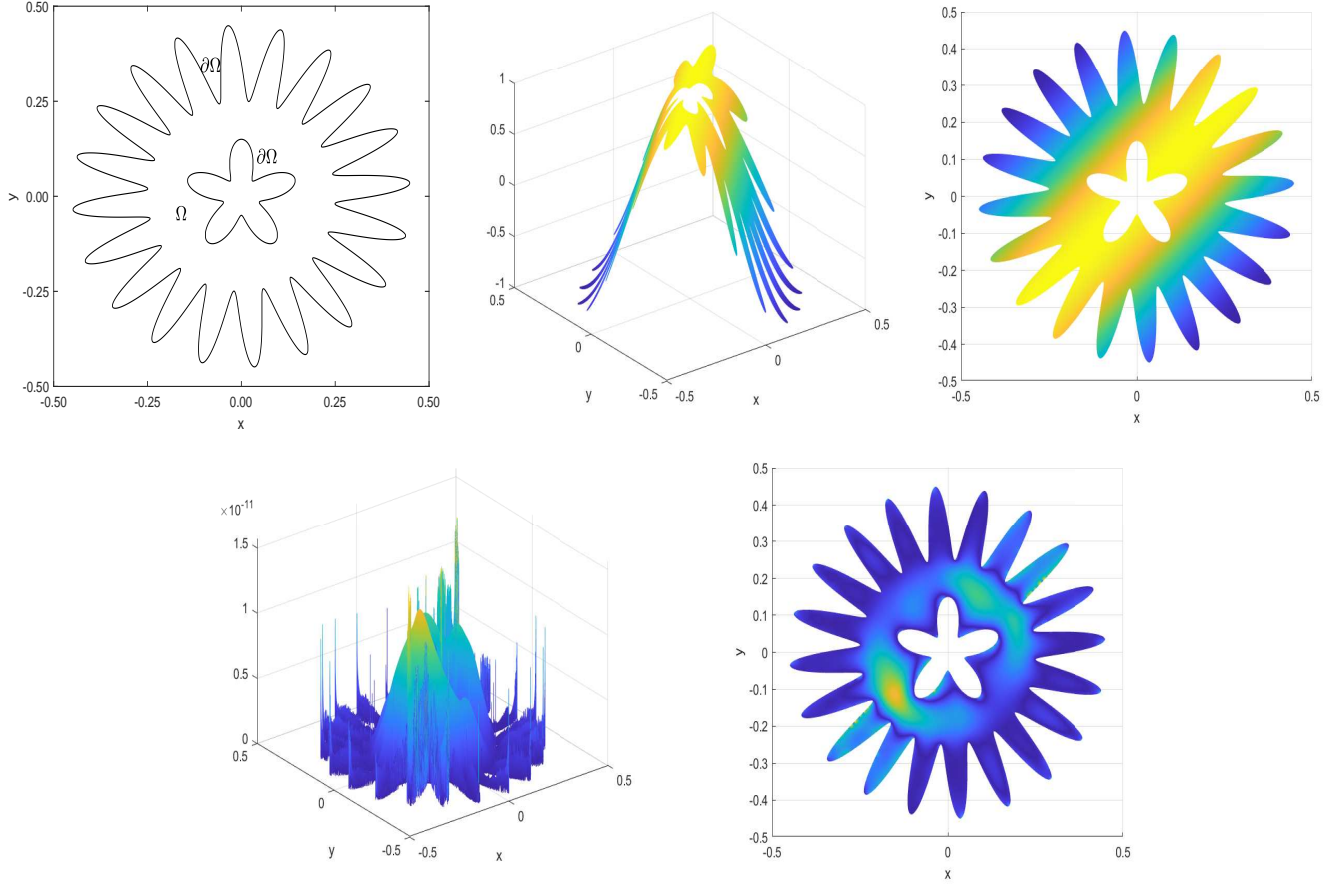


FIGURE 15. Performance in Example 4.2 of the proposed fourth-order compact FDM with $u = \cos(5(x - y))$. The domain $\Omega = \{(x(t), y(t)) : [0.1 + 0.05 \sin(5t)]^2 < x(t)^2 + y(t)^2 < [0.35 + 0.1 \sin(20t)]^2, t \in [0, 2\pi)\}$ that is enclosed by 5-leaf and 20-leaf boundary curves $\partial\Omega$ (left panel in the first row), u_h on $\bar{\Omega}_h$ with $h = 1/2^{12}$ (middle and right panels in the first row), and $|u_h - u|$ on $\bar{\Omega}_h$ with $h = 1/2^{12}$ (left and right panels in the second row).

TABLE 3. Performance in Example 4.2 of the proposed fourth-order compact FDM, where $u = \cos(5(x - y))$ and $\Omega = \{(x(t), y(t)) : [0.1 + 0.05 \sin(5t)]^2 < x(t)^2 + y(t)^2 < [0.35 + 0.1 \sin(20t)]^2, t \in [0, 2\pi)\}$.

h	$\frac{\ u_h - u\ _2}{\ u\ _2}$	order	$\ u_h - u\ _\infty$	order
$1/2^6$	1.9442E-02		2.1208E-01	
$1/2^7$	1.0112E-03	4.26	2.4589E-02	3.11
$1/2^8$	2.5933E-07	11.93	2.0397E-06	13.56
$1/2^9$	1.5692E-08	4.05	5.1251E-08	5.31
$1/2^{10}$	9.6204E-10	4.03	3.9733E-09	3.69
$1/2^{11}$	6.3641E-11	3.92	2.4972E-10	3.99
$1/2^{12}$	5.6048E-12	3.51	1.5665E-11	3.99

$$\Omega = \{(x(t), y(t)) : [0.33 + 0.02 \sin(20t)]^2 < x(t)^2 + y(t)^2 < [0.35 + 0.02 \sin(20t)]^2, t \in [0, 2\pi)\},$$

$$\Omega = \{(x(t), y(t)) : [0.33 + 0.02 \sin(40t)]^2 < x(t)^2 + y(t)^2 < [0.35 + 0.02 \sin(40t)]^2, t \in [0, 2\pi)\},$$

$$\Omega = \{(x(t), y(t)) : [0.33 + 0.02 \sin(100t)]^2 < x(t)^2 + y(t)^2 < [0.35 + 0.02 \sin(100t)]^2, t \in [0, 2\pi)\},$$

$$\Omega = \{(x(t), y(t)) : [0.349 + 0.02 \sin(20t)]^2 < x(t)^2 + y(t)^2 < [0.35 + 0.02 \sin(20t)]^2, t \in [0, 2\pi)\},$$

the source term ϕ and the Dirichlet boundary function g are obtained by plugging above functions into (1.1). The numerical results are presented in Tables 4 to 7 and Figs. 16 to 19.

TABLE 4. Performance in Example 4.3 of the proposed fourth-order compact FDM, where $u = \sin(4x) \cos(4y)$ and $\Omega = \{(x(t), y(t)) : [0.33 + 0.02 \sin(20t)]^2 < x(t)^2 + y(t)^2 < [0.35 + 0.02 \sin(20t)]^2, t \in [0, 2\pi)\}$.

h	$\frac{\ u_h - u\ _2}{\ u\ _2}$	order	$\ u_h - u\ _\infty$	order
$1/2^6$	1.1561E-02		4.7770E-02	
$1/2^7$	6.3478E-07	14.15	2.7195E-06	14.10
$1/2^8$	8.3083E-08	2.93	1.7030E-07	4.00
$1/2^9$	5.6609E-09	3.88	1.1265E-08	3.92
$1/2^{10}$	3.9934E-10	3.83	8.8971E-10	3.66
$1/2^{11}$	2.4814E-11	4.01	5.6864E-11	3.97
$1/2^{12}$	1.4931E-12	4.05	3.7550E-12	3.92

TABLE 5. Performance in Example 4.3 of the proposed fourth-order compact FDM, where $u = \sin(10x) \cos(10y)$ and $\Omega = \{(x(t), y(t)) : [0.33 + 0.02 \sin(40t)]^2 < x(t)^2 + y(t)^2 < [0.35 + 0.02 \sin(40t)]^2, t \in [0, 2\pi)\}$.

h	$\frac{\ u_h - u\ _2}{\ u\ _2}$	order	$\ u_h - u\ _\infty$	order
$1/2^7$	3.0546E-02		3.1862E-01	
$1/2^8$	2.7615E-06	13.43	1.6867E-05	14.21
$1/2^9$	1.7321E-07	3.99	5.0266E-07	5.07
$1/2^{10}$	1.1805E-08	3.87	3.1117E-08	4.01
$1/2^{11}$	7.8057E-10	3.92	2.2230E-09	3.81
$1/2^{12}$	5.0312E-11	3.96	1.4953E-10	3.89
$1/2^{13}$	2.9737E-12	4.08	1.0823E-11	3.79

TABLE 6. Performance in Example 4.3 of the proposed fourth-order compact FDM, where $u = \sin(50x) \cos(50y)$ and $\Omega = \{(x(t), y(t)) : [0.33 + 0.02 \sin(100t)]^2 < x(t)^2 + y(t)^2 < [0.35 + 0.02 \sin(100t)]^2, t \in [0, 2\pi)\}$.

h	$\frac{\ u_h - u\ _2}{\ u\ _2}$	order	$\ u_h - u\ _\infty$	order
$1/2^8$	5.7873E-01		6.4646E+00	
$1/2^9$	1.5027E-01	1.95	3.2825E+00	0.98
$1/2^{10}$	4.2131E-03	5.16	1.3816E-01	4.57
$1/2^{11}$	5.3721E-07	12.94	3.2870E-06	15.36
$1/2^{12}$	3.4059E-08	3.98	8.8488E-08	5.22
$1/2^{13}$	2.1544E-09	3.98	5.6768E-09	3.96
$1/2^{14}$	1.3652E-10	3.98	3.7503E-10	3.92

TABLE 7. Performance in Example 4.3 of the proposed fourth-order compact FDM, where $u = \sin(50x) \cos(50y)$ and $\Omega = \{(x(t), y(t)) : [0.349 + 0.02 \sin(20t)]^2 < x(t)^2 + y(t)^2 < [0.35 + 0.02 \sin(20t)]^2, t \in [0, 2\pi)\}$.

h	$\frac{\ u_h - u\ _2}{\ u\ _2}$	order	$\ u_h - u\ _\infty$	order
$1/2^{10}$	1.3975E-02		1.8476E-01	
$1/2^{11}$	1.8983E-03	2.88	1.5374E-02	3.59
$1/2^{12}$	3.0217E-08	15.94	7.9659E-08	17.56
$1/2^{13}$	2.3576E-09	3.68	5.5330E-09	3.85
$1/2^{14}$	1.5499E-10	3.93	3.2938E-10	4.07

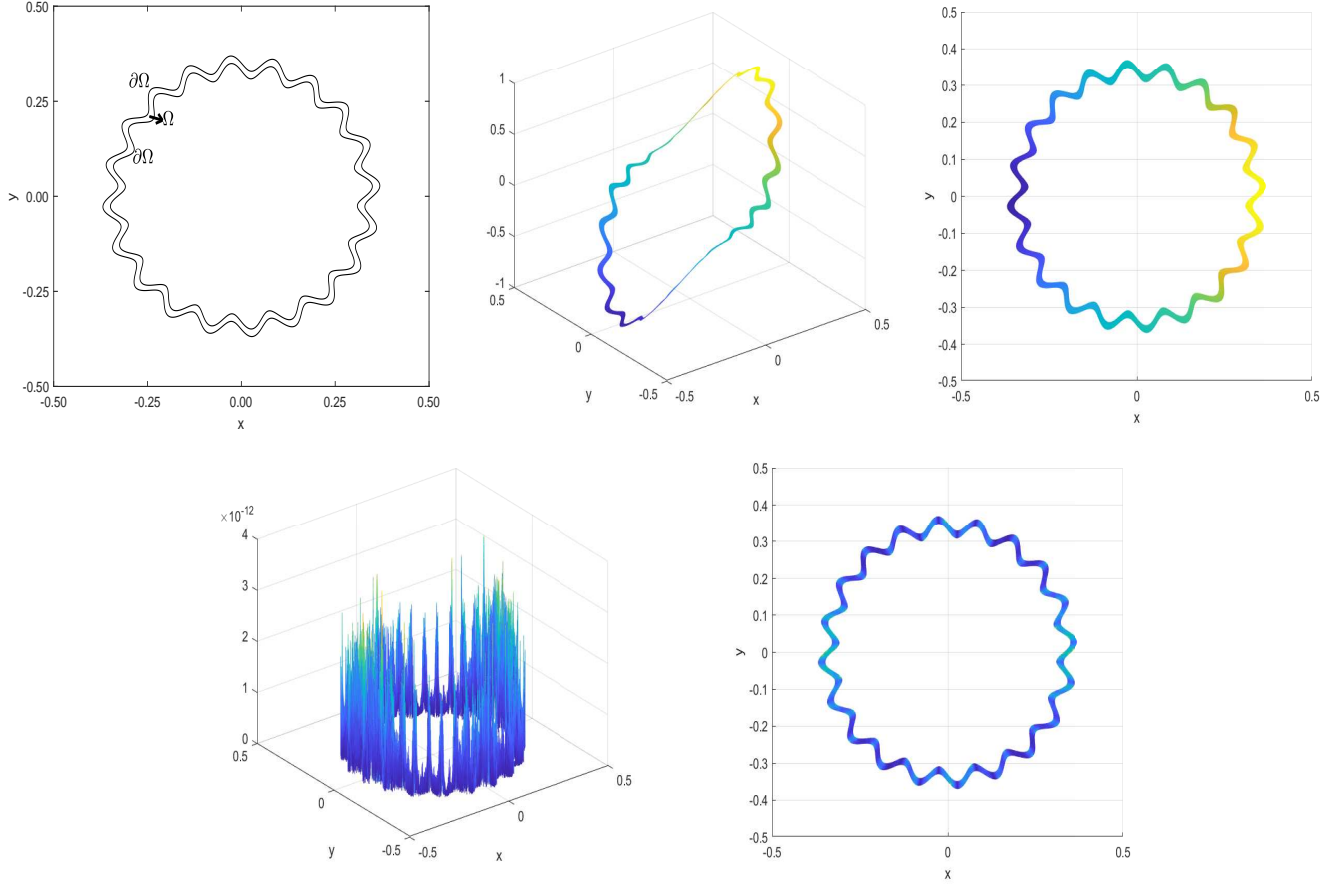


FIGURE 16. Performance in Example 4.3 of the proposed fourth-order compact FDM with $u = \sin(4x) \cos(4y)$. The domain $\Omega = \{(x(t), y(t)) : [0.33 + 0.02 \sin(20t)]^2 < x(t)^2 + y(t)^2 < [0.35 + 0.02 \sin(20t)]^2, t \in [0, 2\pi)\}$ that is enclosed by two 20-leaf boundary curves $\partial\Omega$ (left panel in the first row), u_h on $\bar{\Omega}_h$ with $h = 1/2^{12}$ (middle and right panels in the first row), and $|u_h - u|$ on $\bar{\Omega}_h$ with $h = 1/2^{12}$ (left and right panels in the second row).

5. CONTRIBUTION

In this paper, we consider the convection-diffusion-reaction equation with smooth variable convection, diffusion, reaction functions and the Dirichlet boundary condition on a smooth curved domain. We propose the fourth-order compact FDM to approximate the solution at regular and irregular stencil center points using the uniform Cartesian grid. For the thin domain with the sharply varying boundary curve, there are many configurations of the compact FDM at the irregular stencil center. We establish a linear system with an at most 6×24 matrix to compute the left-hand side of the fourth-order compact FDM to cover all configurations. Furthermore, each entry of the matrix is expressed in the explicit expression for any irregular stencil centers. Once the left-hand side is computed, the right-hand side of the stencil is calculated immediately by the given explicit expression. Strengths of our FDM:

- All formulas are written in explicit forms such that our FDM is simple to be implemented to help readers reproduce our results straightforwardly.
- From numerical examples, our FDM performs well for the boundary curve with the large curvature (e.g. Figs. 13 and 14 and Tables 1 and 2) and the thin domain that cannot be distinguished by the naked eye (e.g. Fig. 19 and Table 7). Our FDM yields the stable convergence rate and the accurate solution for the high-frequency solution and the highly-oscillatory curve (e.g. Fig. 18 and Table 6). Furthermore, all errors are uniformly distributed around the boundary, which demonstrates the stability and robustness of our FDM.

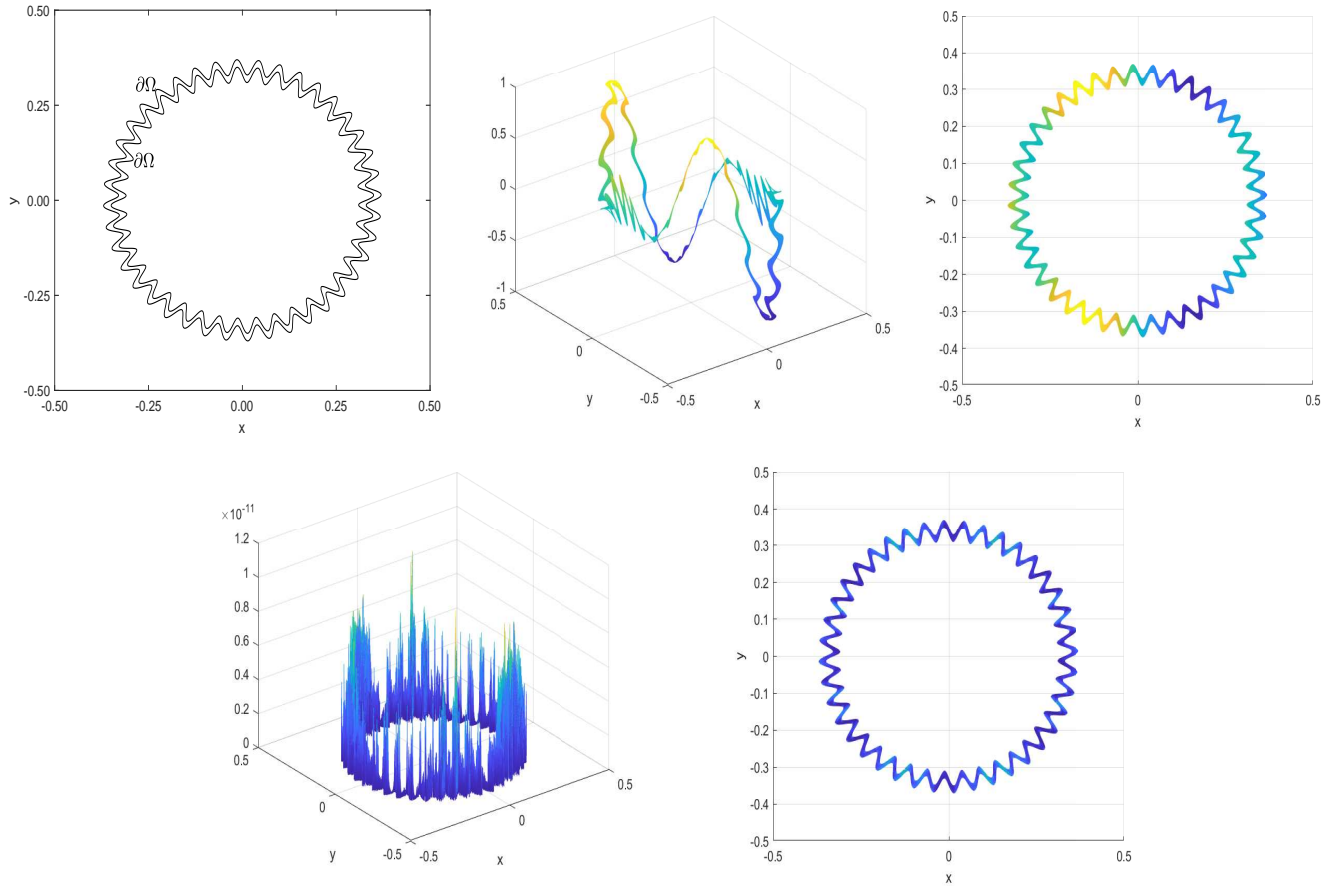


FIGURE 17. Performance in Example 4.3 of the proposed fourth-order compact FDM with $u = \sin(10x) \cos(10y)$. The domain $\Omega = \{(x(t), y(t)) : [0.33 + 0.02 \sin(40t)]^2 < x(t)^2 + y(t)^2 < [0.35 + 0.02 \sin(40t)]^2, t \in [0, 2\pi)\}$ that is enclosed by two 40-leaf boundary curves $\partial\Omega$ (left panel in the first row), u_h on $\bar{\Omega}_h$ with $h = 1/2^{13}$ (middle and right panels in the first row), and $|u_h - u|$ on $\bar{\Omega}_h$ with $h = 1/2^{13}$ (left and right panels in the second row).

- From results in all tables, we observe that the convergence rate is stabilized at 4 when h is reasonably small, which numerically indicates that the convergence of our proposed FDM at the irregular stencil center seems to be independent of the distance between the centered grid point and the boundary curve, or this distance has the limited effect on the accuracy of our FDM.

Key differences from existing methods:

- In contrast to the ghost cell method used in [8, 9], we do not need to use approximated values of u at grid points outside Ω by the interpolation.
- Compared with the immersed interface method (IIM) in [22, 25], we do not utilize the coordinate transformation and solve the optimization problem to obtain the stencil. We use the transformation in Cartesian coordinate directly to achieve the efficient implementation, and solve a small linear system with the explicit expression to compute stencil to improve the accuracy. Furthermore, [22, 25] employ 1 to 4 points at the boundary in the stencil at the irregular stencil center, and we use one point at the boundary to derive the fourth-order compact FDM.
- Distinct from using partial derivatives in the complex field to derive the FDM in [20], we only use the real partial derivatives to build the simple stencil and enhance the efficiency.
- Different from the augmented matched interface and boundary (AMIB) method in [26, 27, 32], we construct the compact scheme which generates a sparse matrix with nine non-zero bands.

The potential of our method:

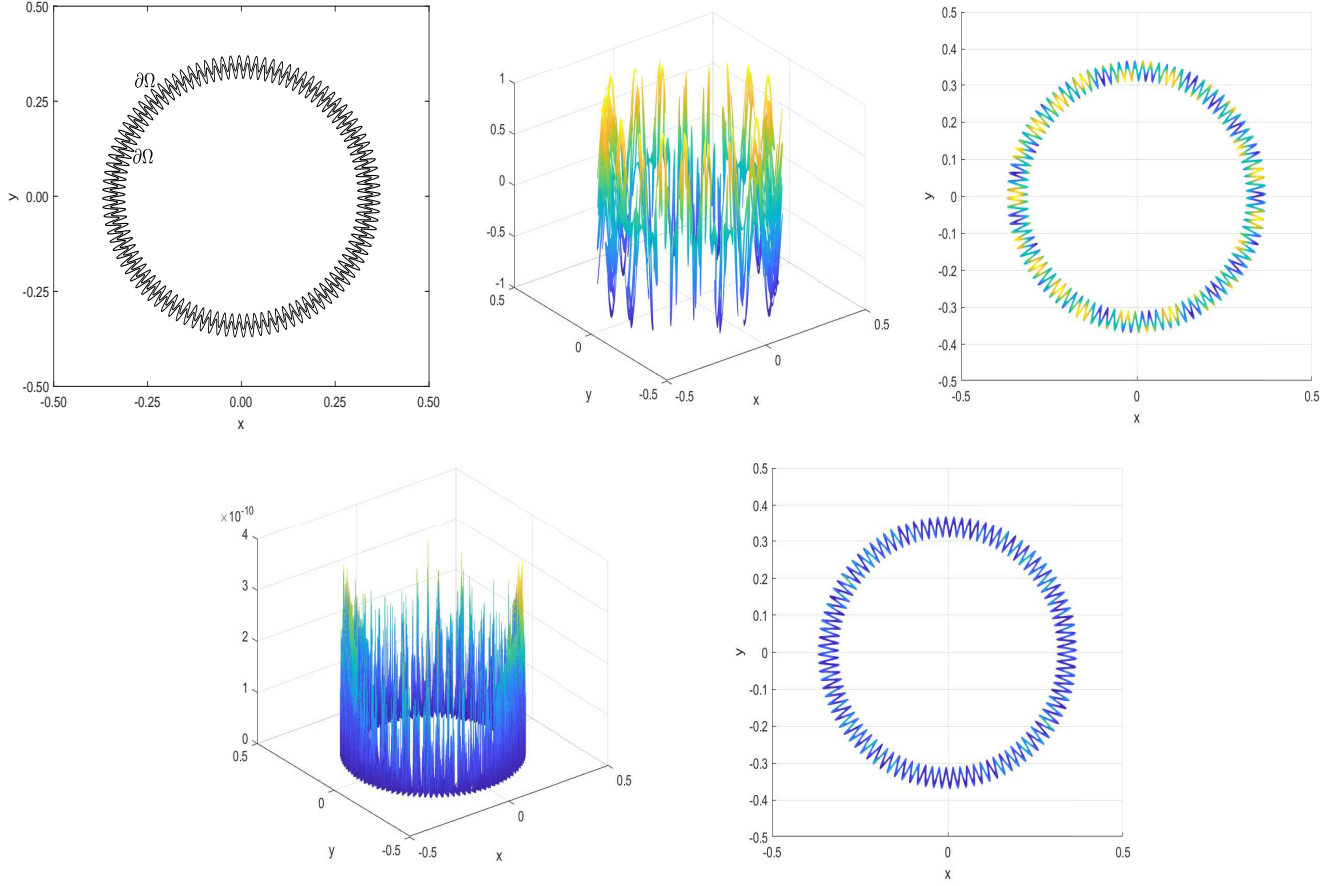


FIGURE 18. Performance in Example 4.3 of the proposed fourth-order compact FDM with $u = \sin(50x) \cos(50y)$. The domain $\Omega = \{(x(t), y(t)) : [0.33 + 0.02 \sin(100t)]^2 < x(t)^2 + y(t)^2 < [0.35 + 0.02 \sin(100t)]^2, t \in [0, 2\pi]\}$ that is enclosed by two 100-leaf boundary curves $\partial\Omega$ (left panel in the first row), u_h on $\bar{\Omega}_h$ with $h = 1/2^{14}$ (middle and right panels in the first row), and $|u_h - u|$ on $\bar{\Omega}_h$ with $h = 1/2^{14}$ (left and right panels in the second row).

- Using techniques in [15, 16], it is direct to extend the proposed fourth-order compact FDM to solve nonlinear steady and unsteady convection-diffusion-reaction equations on irregular domains in 2D and 3D.
- Due to the simple and efficient implementation of our method, it is also straightforward to include more points in the stencil to attain the higher-order accuracy for more challenging PDEs (e.g, the 25-point FDM for the Stokes problem in [14]). Furthermore, it is also feasible to extend our FDM to solve the parabolic equation with the moving boundary/interface and the free boundary problem by the flexibility and efficiency of our derivation.
- We can derive the high-order FDM for (1.1) with Neumann and Robin boundary conditions by replacing (3.2) by $\rho u + \zeta \frac{\partial u}{\partial \bar{n}} = g$ and repeating (3.8)–(3.32) similarly.
- The proposed FDM with more points in the stencil only results in more matrices $A_{r,\ell}$ in the linear system (3.29). So the high-order FDM with the adaptive mesh can be derived easily by adding more $A_{r,\ell}$ in (3.29) for the irregular stencil center near the sharply varying boundary curve.

6. DECLARATIONS

Conflict of interest: The authors declare that they have no conflict of interest.

Data availability: Data will be made available on reasonable request.

Acknowledgment

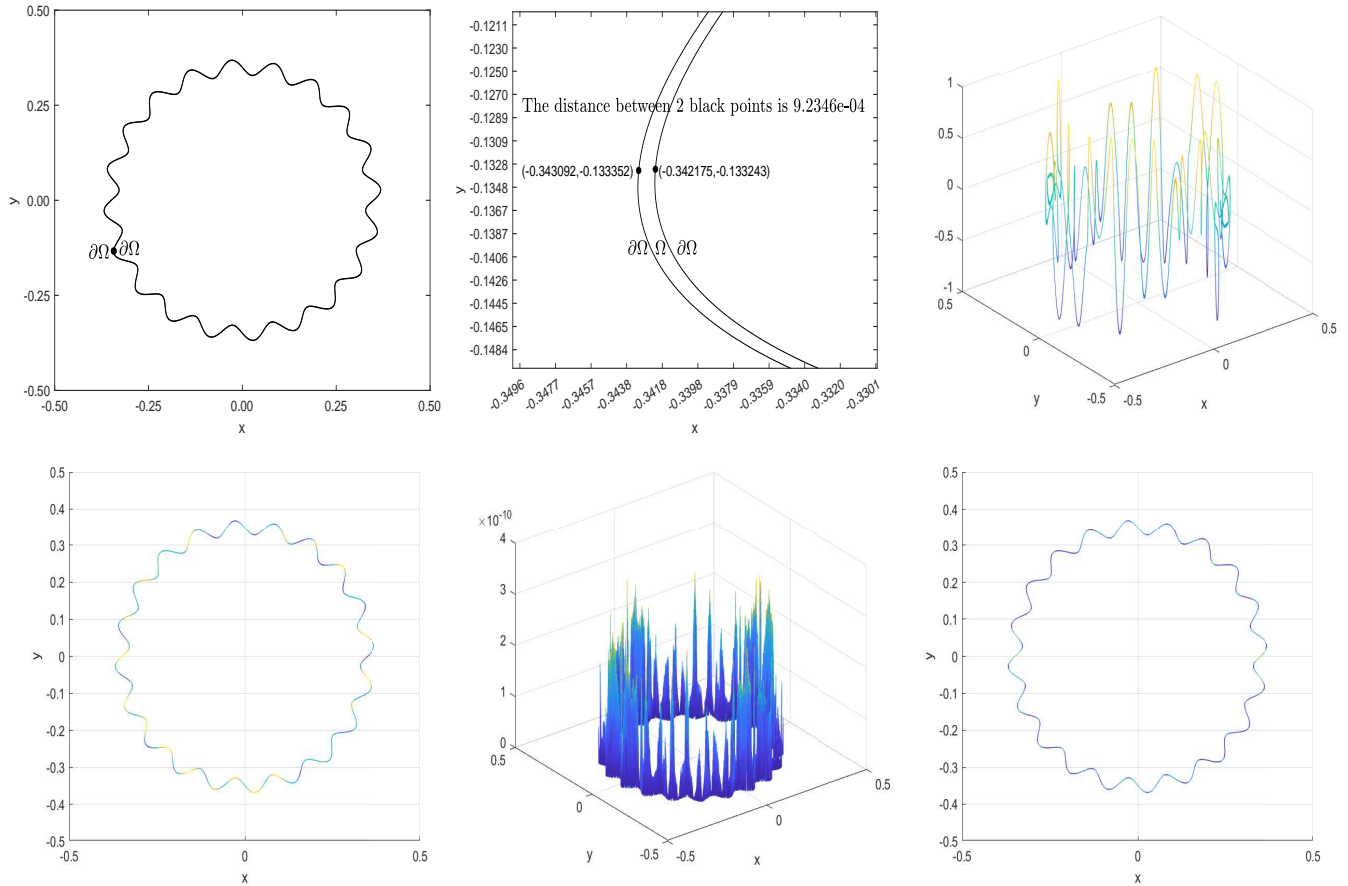


FIGURE 19. Performance in Example 4.3 of the proposed fourth-order compact FDM with $u = \sin(50x) \cos(50y)$. The domain $\Omega = \{(x(t), y(t)) : [0.349 + 0.02 \sin(20t)]^2 < x(t)^2 + y(t)^2 < [0.35 + 0.02 \sin(20t)]^2, t \in [0, 2\pi]\}$ that is enclosed by two nearly overlapping 20-leaf boundary curves $\partial\Omega$ (left and middle panels in the first row), u_h on $\bar{\Omega}_h$ with $h = 1/2^{14}$ (right panel in the first row and left panel in the second row), and $|u_h - u|$ on $\bar{\Omega}_h$ with $h = 1/2^{14}$ (middle and right panels in the second row).

Qiwei Feng is partially supported by the Mathematics Department, King Fahd University of Petroleum and Minerals (KFUPM), Dhahran, Saudi Arabia.

Bin Han is partially supported by Natural Sciences and Engineering Research Council (NSERC) of Canada under grants RGPIN-2024-04991.

The main idea of this manuscript was developed in 2021. Owing to various reasons, the work was delayed. Regrettably, the manuscript was not completed before the third author Peter Minev left us.

REFERENCES

- [1] V. Arias, D. Bochkov, and F. Gibou, Poisson equations in irregular domains with Robin boundary conditions—solver with second-order accurate gradients. *J. Comput. Phys.* **365** (2018), 1-6.
- [2] M. B-Artzi, I. Chorev, J-P. Croisille, and D. Fishelov, A compact difference scheme for the biharmonic equation in planar irregular domains. *SIAM J. Numer. Anal.* **47** (2009), 3087-3108.
- [3] A. Baeza, P. Mulet, and D. Zorío, High order boundary extrapolation technique for finite difference methods on complex domains with Cartesian meshes. *J. Sci. Comput.* **66** (2016), 761-791.
- [4] G. Berikelashvili, M. M. Gupta, and M. Mirianashvili, Convergence of fourth order compact difference schemes for three-dimensional convection-diffusion equations. *SIAM J. Numer. Anal.* **45** (2007), 443-455.
- [5] M. Chai, K. Luo, H. Wang, S. Zheng, and J. Fan, Imposing mixed Dirichlet-Neumann-Robin boundary conditions on irregular domains in a level set/ghost fluid based finite difference framework. *Comput. Fluids.* **214** (2021), 104772.
- [6] G. Chen, Z. Li, and P. Lin, A fast finite difference method for biharmonic equations on irregular domains and its application to an incompressible Stokes flow. *Adv. Comput. Math.* **29** (2008), 113-133.

- [7] H. Chen, C. Min, and F. Gibou, A supra-convergent finite difference scheme for the Poisson and heat equations on irregular domains and non-graded adaptive Cartesian grids. *J. Sci. Comput.* **31** (2007), 19-60.
- [8] S. Clain, D. Lopes, and R. M. S. Pereira, Very high-order Cartesian-grid finite difference method on arbitrary geometries. *J. Comput. Phys.* **434** (2021), 110217.
- [9] S. Clain, D. Lopes, R. M. S. Pereira, and P. A. Pereira, Very high-order finite difference method on arbitrary geometries with Cartesian grids for non-linear convection diffusion reaction equations. *J. Comput. Phys.* **498** (2024), 112667.
- [10] H. Ding, C. Shu, and Q. D. Cai, Applications of stencil-adaptive finite difference method to incompressible viscous flows with curved boundary. *Comput. Fluids.* **36** (2007), 786-793.
- [11] A. Ditkowski, and Y. Harness, High-order embedded finite difference schemes for initial boundary value problems on time dependent irregular domains. *J. Sci. Comput.* **39** (2009), 394-440.
- [12] Q. Feng, B. Han, and M. Michelle, Sixth order compact finite difference method for 2D Helmholtz equations with singular sources and reduced pollution effect. *Commun. Comput. Phys.* **34** (2023), 672-712.
- [13] Q. Feng, B. Han, and P. Mineev, Sixth order compact finite difference schemes for Poisson interface problems with singular sources. *Comp. Math. Appl.* **99** (2021), 2-25.
- [14] Q. Feng, B. Han, and M. Neilan, A high-order, pressure-robust, and decoupled finite difference method for the Stokes problem. *Math. Comput. Simul.* **241** (2026), 634-649.
- [15] Q. Feng and C. Trenchea, Fourth-order compact finite difference methods for nonlinear convection-diffusion equations. *J. Comput. Phys.* **555** (2026), 114783.
- [16] Q. Feng, Fourth-order compact finite difference methods for 2D and 3D nonlinear convection-diffusion-reaction equations. Preprint, 2026. <https://arxiv.org/abs/2603.16226>.
- [17] J. F-Fidalgo, S. Clain, L. Ramírez, I. Colominas, and X. Nogueira, Very high-order method on immersed curved domains for finite difference schemes with regular Cartesian grids. *Comput. Methods Appl. Mech. Engrg.* **360** (2020), 112782.
- [18] F. Gibou and R. Fedkiw, A fourth order accurate discretization for the Laplace and heat equations on arbitrary domains, with applications to the Stefan problem. *J. Comput. Phys.* **202** (2005), 577-601.
- [19] F. Gibou, R. P. Fedkiw, L-T. Cheng, and M. Kang, A second-order-accurate symmetric discretization of the Poisson equation on irregular domains. *J. Comput. Phys.* **176** (2002), 205-227.
- [20] B. Han and J. Sim, Convergent sixth-order compact finite difference method for variable-coefficient elliptic PDEs in curved domains. *J. Sci. Comput.* **104** (2025), 66, 1-46.
- [21] Á. Helgadóttir and F. Gibou, A Poisson-Boltzmann solver on irregular domains with Neumann or Robin boundary conditions on non-graded adaptive grid. *J. Comput. Phys.* **230** (2011), 3830-3848.
- [22] K. Ito, Z. Li, and Y. Kyei, Higher-order, Cartesian grid based finite difference schemes for elliptic equations on irregular domains. *SIAM J. Sci. Comput.* **27** (2005), 346-367.
- [23] Z. Jomaa and C. Macaskill, The embedded finite difference method for the Poisson equation in a domain with an irregular boundary and Dirichlet boundary conditions. *J. Comput. Phys.* **202** (2005), 488-506.
- [24] M. Lakner and I. Plazl, The finite differences method for solving systems on irregular shapes. *Comput. Chem. Eng.* **32** (2008), 2891-2896.
- [25] Z. Li and K. Ito, The Immersed Interface Method: Numerical Solutions of PDEs Involving Interfaces and Irregular Domains, *Frontiers in Applied Mathematics. Society for Industrial and Applied Mathematics.* 2006.
- [26] C. Li, Y. Ren, G. Long, E. Boerman, and S. Zhao, A fast sine transform accelerated high-order finite difference method for parabolic problems over irregular domains. *J. Sci. Comput.* **95** (2023), 49, 1-38.
- [27] C. Li, S. Zhao, B. Pentecost, Y. Ren, and Z. Guan, A spatially fourth-order Cartesian grid method for fast solutions of elliptic and parabolic problems on irregular domains with sharply curved boundaries. *J. Sci. Comput.* **103** (2025), 94, 1-35.
- [28] T. Liszka and J. Orkisz, The finite difference method at arbitrary irregular grids and its application in applied mechanics. *Comput. Struct.* **11** (1980), 83-95.
- [29] Y. T. Ng, H. Chen, C. Min, and F. Gibou, Guidelines for Poisson solvers on irregular domains with Dirichlet boundary conditions using the ghost fluid method. *J. Sci. Comput.* **41** (2009), 300-320.
- [30] P. Olsson, High order finite differences methods on non-smooth domains. *Comput. Methods Appl. Mech. Engrg.* **116** (1994), 265-272.
- [31] K. Pan, D. He, and Z. Li, A high order compact FD framework for elliptic BVPs involving singular sources, interfaces, and irregular domains. *J. Sci. Comput.* **88** (2021), 67, 1-25.
- [32] Y. Ren, H. Feng, and S. Zhao, A FFT accelerated high order finite difference method for elliptic boundary value problems over irregular domains. *J. Comput. Phys.* **448** (2022), 110762.
- [33] Y. Shi, S. Xie, D. Liang, and K. Fu, High order compact block-centered finite difference schemes for elliptic and parabolic problems. *J. Sci. Comput.* **87** (2021), 86, 1-26.
- [34] M. Theillard, L. F. Djodom, J-L. Vié, and F. Gibou, A second-order sharp numerical method for solving the linear elasticity equations on irregular domains and adaptive grids-application to shape optimization. *J. Comput. Phys.* **233** (2013), 430-448.

- [35] G. Yoon and C. Min, Analyses on the finite difference method by Gibou et al. for Poisson equation. *J. Comput. Phys.* **280** (2015), 184-194.
- [36] S. M. Zhang and Z. Li, An augmented IIM for Helmholtz/Poisson equations on irregular domains in complex space. *Int. J. Numer. Anal. Model.* **13** (2016), 166-178.

MATHEMATICS DEPARTMENT, KING FAHD UNIVERSITY OF PETROLEUM AND MINERALS, DHAHRAN, 31261, SAUDI ARABIA.

Email address: `qiwei.feng@kfupm.edu.sa, qfeng@ualberta.ca`

DEPARTMENT OF MATHEMATICAL AND STATISTICAL SCIENCES, UNIVERSITY OF ALBERTA, EDMONTON, ALBERTA, CANADA T6G 2N8.

Email address: `bhan@ualberta.ca minev@ualberta.ca`